geotechnics

MDPI

Article

Development of Soil Moisture Content and Soil Matric Suction Model Based on Field Instrumentation and Electrical Resistivity Imaging (ERI) for Highway Slopes Constructed on High Expansive Clay Soil

Masoud Nobahar *, Rakesh Salunke, Mohammad Sadik Khan * and Farshad Amini

Department of Civil and Environmental Engineering, Jackson State University, 1400 J.R. Lynch Street, Jackson, MS 17068, USA

* Correspondence: j00816771@students.jsums.edu (M.N.); j00797693@jsums.edu (M.S.K.)

Abstract: In highway slopes (HWS) constructed on high expansive clay soil (HECS), in situ moisture variation is an environmentally driven variable that can significantly impact the safety of the constructed soil. Electrical resistivity imaging (ERI) is a non-destructive method with a considerable potential for subsurface soil moisture mapping, which can be correlated with volumetric soil moisture content (VSMC) and soil matric suction (SMS) of HECS to remarkably enhance the evaluation of the performance of the HWS. However, limited datasets are available to evaluate the accuracy and feasibility of the available correlative field-based models for the HECS under various field conditions. The objective of the current study is to develop a field-based model of VSMC and SMS using real-time field monitoring and ERI data. Six HWS located in the Jackson metro area in Mississippi (MS), USA were considered as reference slopes in this study. Comprehensive field instrumentation was executed at the six HWS to monitor the VSMC, SMS and rainfall intensity. The sensors were installed at the crest, middle and toe of the slope. The 2D ERI test was conducted using a dipole–dipole array with multiple electrodes at 5 ft (1.5 m) spacing. The ERI survey was conducted at the crest and middle of the six HWS to image the continuous soil subsurface profile in terms of moisture variation. The developed models indicated a good agreement between instrumented and ERI data. The developed models will facilitate the estimation of VSMC and SMS variations and aid in performance monitoring of the HWS built on HECS such as Yazoo clay.

Keywords: highway slope; expansive clay; field instrumentation; electrical resistivity imaging

Citation: Nobahar, M.; Salunke, R.; Khan, M.S.; Amini, F. Development of Soil Moisture Content and Soil Matric Suction Model Based on Field Instrumentation and Electrical Resistivity Imaging (ERI) for Highway Slopes Constructed on High Expansive Clay Soil. *Geotechnics* **2022**, *2*, 671–705. https://doi.org/10.3390/geotechnics2030033

Academic Editors: Yong Sheng and Abbas Taheri

Received: 29 June 2022
Accepted: 13 August 2022
Published: 17 August 2022

1. Introduction

Highway slopes (HWS) constructed with high expansive clay are prone to substantial cyclic swelling and shrinking as a result of soaking and drying cycles, compromising the slopes' stability. The risk is further exacerbated when rainwater infiltrates the surface and the upper layers of the HWS, decreasing the soil matric suction (SMS) within the unsaturated soil mass. Negative pore water pressure (SMS capacity) is strong within the unsaturated zone at the surficial levels of an HWS, which stabilizes the HWS and avoids shallow HWS failures. Increased rainfall intensity can instantly raise the saturation level, hence raising pore water pressure and decreasing the SMS capacity of the HWS surface, resulting in HWS instability [1–4].

Electrical resistivity imaging (ERI) is a non-destructive technology used to investigate and characterize soils. The technology enables rapid research of the subsurface of larger areas compared to that investigated by destructive penetrometer testing methods such as cone penetration test (CPT) and standard penetration test (SPT). Furthermore, ERI is a relatively less expensive technique of subsurface investigation compared to its destructive counterparts, especially considering the vast areas investigated. Due to the limited

accessibility of the drill rig on sloping terrain, soil test boring is typically limited in extent. Electrical resistance (ER) varies depending on the characteristics of the soil [5–7]. The nature of the solid elements, the configuration of the voids, the degree of water saturation, the ER of the fluid and the temperature all contribute to the soil's ER [8,9]. The air medium acts as a resistive insulator indefinitely, whereas the water solution serves as a conductor. A substance's electrical resistance is proportional to its ionic concentration. Solid grain ER is proportional to the density of the electrical charges on the surface of the soil particles. ER is a property of soil that is determined by its characteristics, yet it varies considerably in terms of direction and magnitude [10,11]. ER measurements were used to map the soil and produced a wide variety of results. The ER of saline water in dry soil over crystalline rocks ranges from 3.2 ft (0.97 m) to 344.4 ft (104.8 m) [10]. ERI may be used in the field to measure the degree of saturation, moisture content and clay content, according to a recent study [12]. However, the ERI technique is severely limited in its use of measuring soil data, owing to the lack of a model connecting the soil data to geophysics. Numerous investigations have been carried out to determine the ER as a function of the pore fluid's conductivity and the surface conductance [10,13–16]. However, a general model explaining the link between electrical conductivity and soil characteristics does not exist due to the inherent complexity of the soil water matrix and the interdependence of major components. Archie [13] developed an empirical formula to correlate the bulk resistivity of saturated soil with pore fluid resistivity and porosity. If the resistivity of soil is ρ, the resistivity of pore fluid is ρ_w and porosity is n, then Archie's formula can be stated in Equation (1) as:

$$\rho = a\ (\rho_w)\ n^{-m} \tag{1}$$

where a and m are the fitting and cementation parameters, respectively, according to the study, and the value of m depends on the interconnectivity of the pore network and tortuosity. In an unsaturated media, Archie's law [13] can be presented in Equation (2) as:

$$\rho = a\ (\rho_w)\ n^{-m}\ S^{-B} \tag{2}$$

where S is the degree of saturation and B is an empirical parameter (averaged 2) called the Archie saturation exponent. B depends on the distribution of the conductive fluid throughout the porous medium and therefore it is not a single-valued function of saturation.

Sauer [14] suggested the flow of current through soils using a three-element network model. According to the authors, current flows through surface charge and pore fluid along with a combined series and parallel paths in clayey soils. The conductivity of a clayey particulate media (σ) can be described by Equation (3) as:

$$\sigma = \frac{a\ (\sigma_s)\ (\sigma_W)}{(1-e)\ (\sigma_W) + e\ (\sigma_s)} + b\ (\sigma_s) + c\ (\sigma_W) \tag{3}$$

where σ_s is the surface conductance, σ_w is the pore water conductivity and constants a, b, c, d and e are functions of porosity and degree of saturation.

Waxman and Smits [15] developed a simplified model where the series effects of surface conductance and pore fluid conductivity were not considered. The contribution of the series path was substituted by a constant surface conductance. The system was equivalent to a circuit composed of two resistors connected in a parallel direction. Therefore, the proposed expression is known as the two parallel resistor model. According to the model, the electric conductivity of soil (σ) can be expressed by Equation (4) as:

$$\sigma = X\ (\sigma_s + (\sigma_W)) \tag{4}$$

where X is a constant that is reciprocal to the formation factor.

Shah and Singh [16] suggested a generalized form of Archie's law for fine-grained soil. According to the authors, the effect of surface conductivity can be included in the cementa-

tion factor of Archie's law. Hence, the proposed relationship in terms of conductivity can be presented by Equation (5) as:

$$\sigma = c\ (\sigma_w)\ \theta^m \tag{5}$$

where $c = 1.45$ when CL < 5% and $c = 0.6\ CL^{0.55}$ when CL $\geq$ 5%, $m = 1.25$ when CL < 5% and $m = 0.92\ CL^{0.2}$ when CL $\geq$ 5%, σ is bulk conductivity of soil, σ_w is pore-water conductivity, θ is volumetric soil moisture content (VSMC) and CL is a percentage of clay fraction in the soil.

Additionally, the association between ERI and SMS models for certain HWS can be beneficial for establishing a warning system for future slides based solely on ERI data. Additionally, attempts to quantify slide failures using quantitative numerical methodologies have demonstrated that correct results are only possible under certain conditions when the geology, strength and hydraulic characteristics of the HWS are completely understood [17]. It will be possible to construct a two-dimensional SMS profile of soil using a model that correlates ER with SMS. At the moment, only water potential sensors (tensiometers) may be planted in the ground to collect real-time data on SMS fluctuation. By establishing a relationship between the ER imaging technique and the SMS, it is possible to generate SMS variation within the soil (2D and 3D). However, there are just a few studies that attempt to bridge the divide between ER imaging and SMS variation in the literature [18–20].

Variation in moisture and infiltration, as well as temperature variation, can be detrimental to slopes constructed on expansive clay soil. Moisture content has an effect on soil qualities, which in turn has an effect on the soil cohesion, which in turn has an effect on the soil layers. As a result, it is critical to monitor the earth slopes constructed on expansive clay soil to gain a better understanding of these actions and their consequences [21]. Moisture fluctuates between slope expansive soil layers and its effects are more pronounced in the weathered soil layer than in the un-weathered ones [22]. In contrast, temperature fluctuations have a lesser effect on the deeper layers (subgrade). On-site Instrumentation and monitoring are critical for observing these impacts [23]. Moisture and temperature changes work together to distort, crack and roughen the expansive soil layers [24]. Moisture and temperature sensors, water potential probes, rain gauges, surveying points, inclinometer profiling, resistivity imaging and ground-penetrating radars are frequently used to observe the impacts of moisture and temperature on deformation, cracking and increased roughness [3]. Specific instruments and related material are discussed in the following subsections.

Even though the sensors are providing the real-time information of the HWSs, it is not always possible for the DOTs to instrument the critical HWSs. In addition, the sensors give point information, which in many cases gives limited information and misses the big picture of the HWSs. These short comings of the evaluation of the sensors can be significantly improved by combing the 2D geophysical testing, such as 2D ERI, which will be instrumental to evaluate the HWS and reducing the risk. For example, in case of landslide evaluation and mitigation, knowing the influence area of the perched water zone and depth of the failure at the field level will significantly improve the landslide repair design, enhance safety, performance and cost-effectiveness. Additional monitoring of the field performance of the instrumented HWS will improvise the understanding of the long-term behavior of moisture intrusion, development of perched water zone and seasonal moisture and matric suction changes, which overall leads to the sustainability and resiliency of the monitored referenced HWSs. During this research study, geophysical research data were obtained and analyzed for six HWS, several of which failed, all of which were constructed on expansive Yazoo clay in and around the Jackson, MS metro region. VSMC and SMS fluctuation data were obtained using automated soil moisture sensors and water potential probes positioned at the HWS. ERI tests were performed on each of the HWS at two distinct intervals and resistivity imaging data were recorded. The interdependencies are studied using geophysical data from the ERI, soil moisture data from field equipment and SMS variation data from field instrumentation. Additionally, the idea of developing a model based on dependability to forecast SMS capacity using ERI tomography data is investigated.

2. Site Selection and Characteristics

This study examined six HWS constructed using high plastic Yazoo clay in and around the Jackson, MS Metropolitan Area. The locations of the sites are depicted in Figure 1 and will be investigated separately in the following sections. Six HWS in the Jackson Metropolitan Area were chosen for this study (Figure 1). The selected HWS have a documented history of failure and repair and most of them have an unstable section that has witnessed deformations.

Index	HWS	Site Location
#1	1	Slope near I220N Ramp toward I55N
#2	2	Slope along I220 N over US 80 near Metro Center
#3	3	Slope along Terry Road/I20 Interchange
#4	4	Slope along I20 over Highland drive
#5	5	Slope near Sowell road/I55S interchange
#6	6	Slope along I20WB near McRaven Road and highway 18

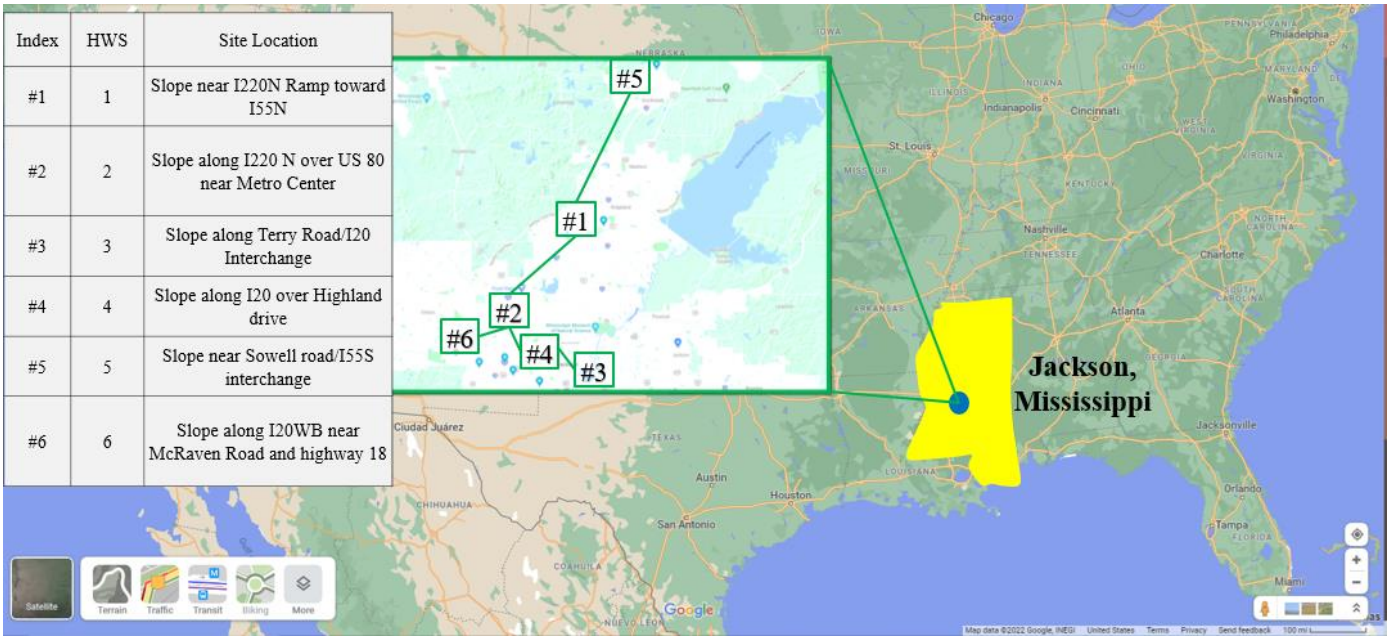

Figure 1. Site Locations of HWS.

HECS Soil (Yazoo Clay) Physical Properties

Representative Yazoo clay samples were collected from the six HWS at different depths up to 30 ft (9.1 m). The samples were from either a stable area or an area susceptible to failure. An estimate of the plasticity index is necessary to classify the soils, particularly in highly expansive clays. Figure 2 shows the Atterberg limits (liquid limit (LL) and plastic limit (PL)) derived from the lab investigation. It is evident that the majority of the collected soil samples have a high range of LL and PL, showing a high plastic characteristic. Furthermore, these consistency limits are valuable in understanding the soil's stress history and general properties.

The hydrometer test was performed according to ASTM D7928-17 test method. The combined particle size distribution curve of the Yazoo clay soil is presented in Figure 3.

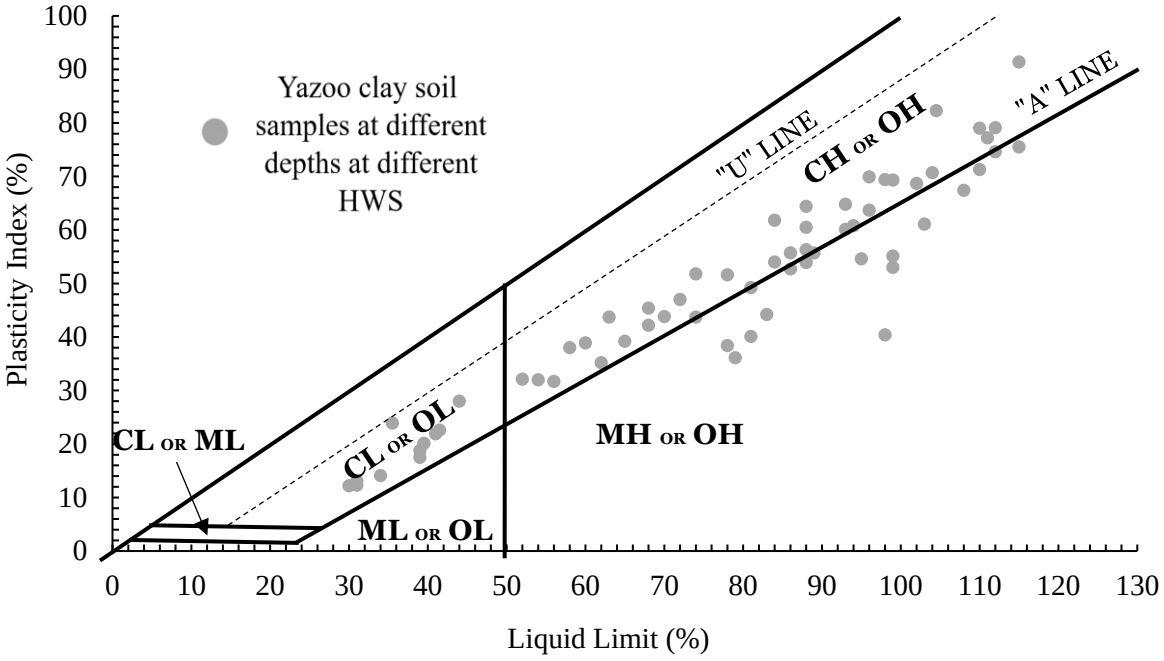

Figure 2. Atterberg limits test results.

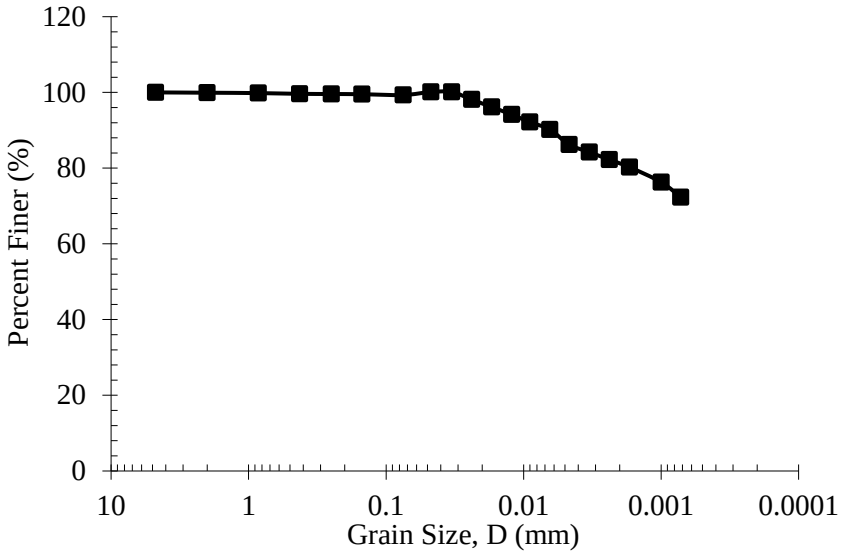

Figure 3. Combined particle size distribution curve of Yazoo clay.

3. Methodology

The methodology adopted in this study is presented in the form of a flowchart in Figure 4. It consisted of four stages: data collection followed by data processing, analysis and data modeling. In the data collection stage, SMC, SMS and precipitation data were collected from the six instrumented HWS using an in situ data logger. ERI tests were performed on each HWS and resistivity imaging data were recorded. The connections between ERI and observed VSMC and SMS from instrumentation are studied in the data analysis stage. In the data modeling stage, multiple models were developed based on interdependencies between ERI vs. SMC and SMS. These models were further evaluated to investigate their potential to forecast SMC and SMS capacities using ERI tomography data.

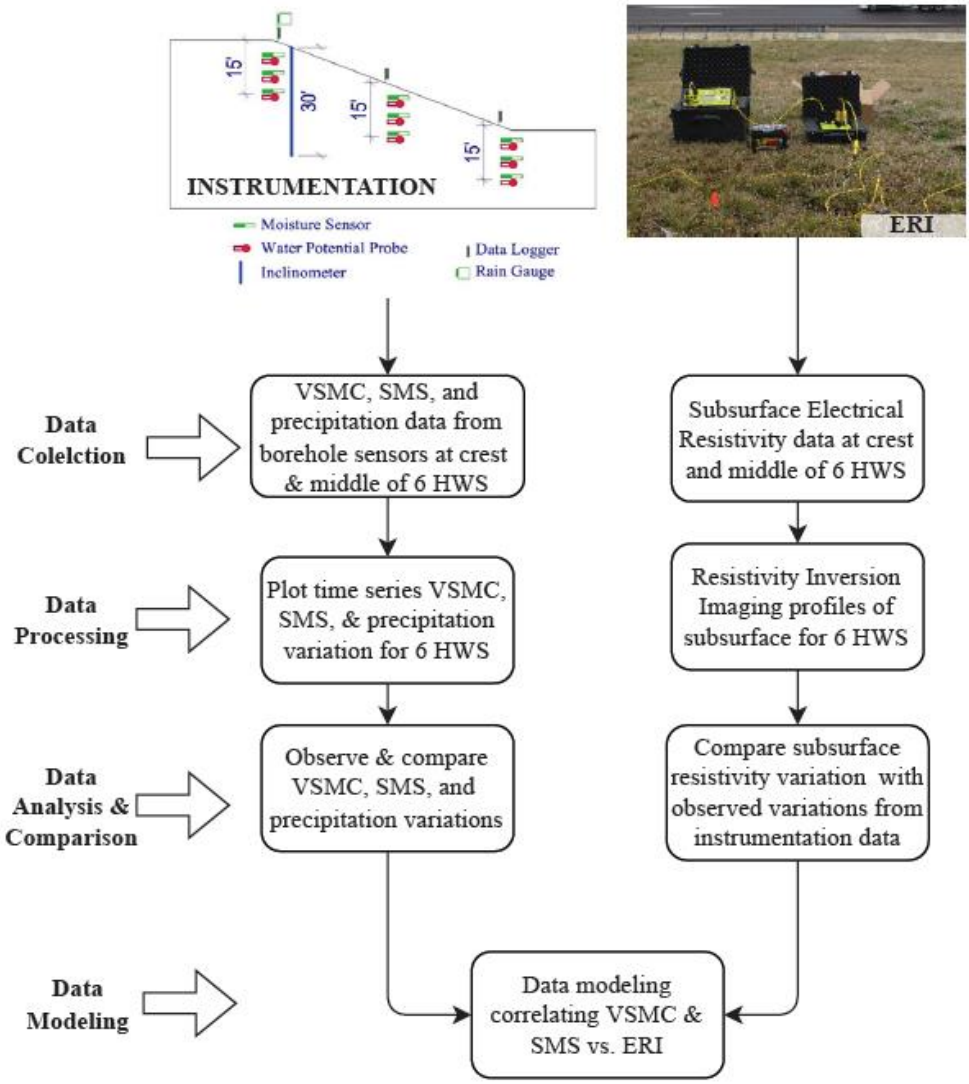

Figure 4. Current study guideline flowchart.

4. Field Instrumentation

The VSMC, SMS and rainfall intensity were all measured on the six slopes using extensive field instruments. Additionally, two 30 ft (10 m)-long inclinometer casing pipes were placed to monitor the slopes' movement. Sensors were put at the top, middle and bottom of the slope. Moisture and water potential sensors were installed in three 15 ft (3 m) deep boreholes at depths of 5 ft (1.5 m), 10 ft (3 m) and 15 ft (5 m) (Figure 4). It should be noted that the types of the instrumentation are as follows; VSMC (Type: GS1-Decagon Devices), SMS (Type: Teros 21 (MPS6)-Meter Group), rain gauge (Type: ECRN-50-Meter Group) and data logger (Type: Em50-Meter Group). The instrumentation configuration for a typical HWS site is depicted in Figure 5. Moisture sensors and water potential probes were put within the HWS and data were collected biweekly from sites. At 5 ft (1.5 m), 10 ft (3 m) and 15 ft (5 m) depths, the VSMC and SMS (water potential) were determined. Furthermore, instrumentation readings were taken at the HWS' crest, middle and toe. Only data collected at the crest and center of the HWS were considered for this investigation. Additionally, ERI research was undertaken on each of the six HWS. The ERI investigations were conducted at the crest and middle of the six HWS. The ERI survey lines spanned approximately 270 ft (82 m) across each of the six HWS surfaces. The electrodes were spaced at around 5 ft (1.5 m) distance and resistivities of the subsoil were recorded at a depth of at least 15 ft (5 m) and up to 65 ft (19 m).

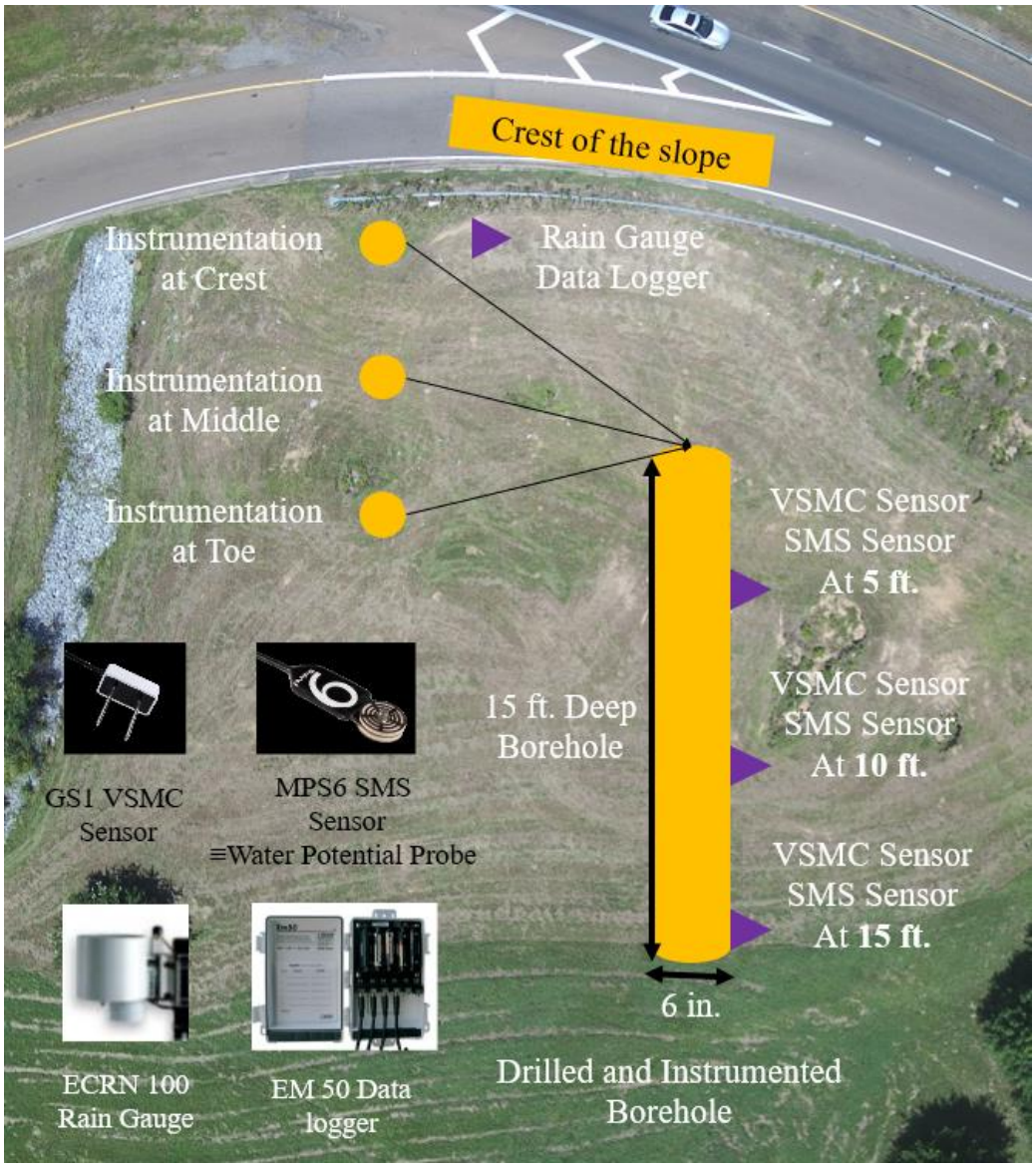

Figure 5. Typical Instrumentation locations on a HWS (Drone Image-top view) (1′ = 1 ft = 0.305 m).

Soil Moisture Sensor Calibration

This study employed a practical calibration methodology [25]. At the HWS, undisturbed soil samples were gathered at various depths near the instrumentation locations. Soil samples were collected and put into the calibration container. A soil moisture sensor was placed and its readings were recorded at the same depths as the retrieved soil samples.

Using the collected soil samples, VSMC was measured in the lab. The laboratory-measured VSMC was then compared with the sensor-measured volumetric water content, which revealed an excellent correlation. From this comparison, a calibration correlation equation was built using the mathematical model for curve fitting. There was good agreement between laboratory measurements of VSMC and sensor readings of VSMC. The supplied data are best matched by a linear equation, as shown in Figure 6. The linear regression correlation illustrates the validation of laboratory-measured VSMC against that from the sensor readings. After developing the calibration function, it was applied straight to the sensor scaling software.

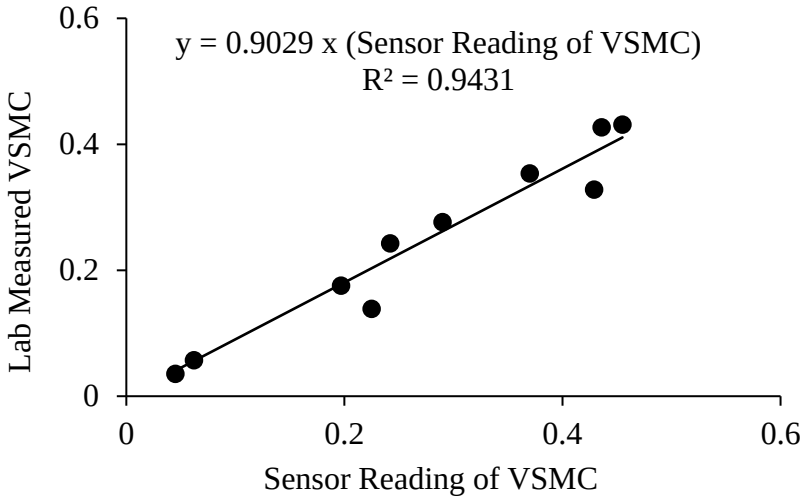

Figure 6. Validation of lab measured vs. sensor reading of VSMC [25].

5. Electrical Resistivity Imaging (ERI)

ERI is a property of a material that indicates how well it resists the flow of electric current. ERI has developed into a promising tool for geophysical exploration. Geophysical surveys conducted by ERI are based on the premise that the earth behaves like a collection of electrical resistors. The potential difference between two sites on the ground can be determined by passing a current through electrodes directly into the ground.

The SI unit for resistivity is the Ohmmeter, abbreviated as Ω.m. Figure 7 depicts the resistivity profile in the ground, as well as the resistivity equipment and arrangement. The electrical resistance of a cylindrical body of length L and cross-sectional area A is denoted by R. Electrical resistance is defined by Ohm's law as the ratio of potential difference to electric current, where *V* denotes the potential (or voltage) difference in volts and I denotes the current in amperes. The voltage (*V*) at the radial distance (*r*) in a homogeneous medium with the current electrode generating I amperes [12]. The ERI field test was conducted utilizing a SuperSting R8/IP resistivity meter from Advanced Geosciences Inc. (AGI) (Figure 6).

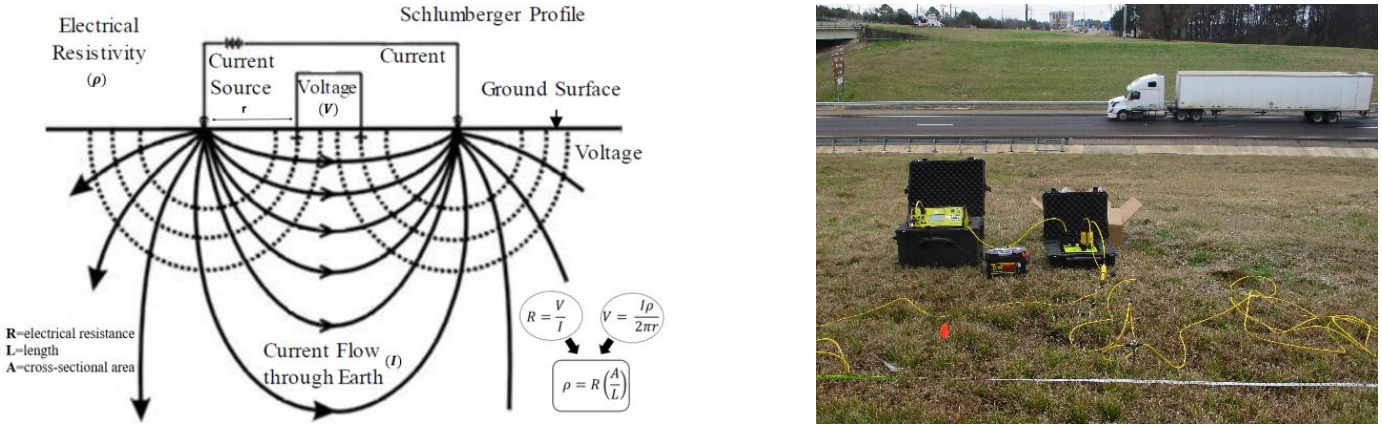

(**a**) (**b**)

Figure 7. (**a**) ERI Subsoil current flow profile [25] (**b**) ERI equipment and field investigation.

The SuperSting R8/IP is a multichannel system with eight survey channels and eight receivers, each of which is capable of taking eight readings for each current injection. The multichannel system made use of a total of 56 electrodes. The SuperSting R8 determines the resistance of the soil body to an electric current sent through it via a line of up to 56 or more electrodes put up to a depth of 6 in (0.15 m) in the ground. The operation begins by

injecting current into the ground from a pair of electrodes at one end of the line electrodes and measuring the potential created by the current at a pair of electrodes adjacent to the first pair. The potential electrodes are then switched to the next pair in line using a built-in switching system within the SuperSting R8 device's microprocessor, while the current electrodes remain in their original positions and the potential difference is then measured.

This procedure is repeated, with many readings taken while repositioning the potential electrodes until the readings dry up. At this point, the current electrodes are moved to the next pair in line and the process of measuring potential difference is repeated in pairs for the remaining electrodes. The cycle is repeated with various configurations of current and potential electrodes. For example, in one design, current electrodes are placed at each end of the line, while potential differences are monitored in pairs between the two electrodes adjacent to the current electrodes.

Numerous studies, including one by Lesparre et al. [26], have established that electrode spacing modifications affect the depth and resolution (quantity and quality of data) of resistivity imaging. For example, increasing electrode spacing allows currents to penetrate deeper into the body but results in a weaker measurement. Reduced spacing improves resolution, but depth is limited. Increased electrode spacing, for example, results in more current penetration to greater depths but produces a weaker reading. Reduced spacing improves resolution but restricts depth. The current work employed 2D resistivity imaging with 56 electrodes spaced 5 ft (1.5 m) center-to-center along 270 ft (82 m) long test lines. Among the several configurations available (Wenner, dipole–dipole and so on), the dipole–dipole array configuration was chosen for this investigation. The dipole–dipole array is optimal for recording horizontal resistivity variations, which made it the obvious choice for this work. Resistivities at various depths are measured by automatically changing the electrode configurations on the Supersting R8. The Superstring R8 is capable of rapidly acquiring thousands of readings at all cycles.

6. Field Testing Results and Data Analysis

6.1. HWS 1

Figure 8 clearly describes HWS1 in terms of its name, location, geometry, history, instrumentation layout and ERI test locations. The failed HWS1 was repaired with a series of deep H-piles. The rebuilt section of the HWS1 is positioned on the east side and the as-built area is located on the west side.

6.1.1. Instrumentation Layout

Deep boreholes were drilled and then instrumented in the repaired area at the crest and middle of the HWS1, which is designated as Instrumentation I, II and III, respectively (Figure 8). Instrumentation I and Instrumentation II are located in the as-built section and Instrumentation III is close to the repaired section. The instrumentations were installed at the repaired and as-built sections with the intention of comparing and studying the variations between the two sections over time. In each of the instrumentation locations, at 5 ft (1.5 m), 10 ft (3 m) and 15 ft (5 m) depths, a moisture sensor and a potential water sensor were installed. Additionally, a rain gauge and air temperature sensor were installed at Instrumentation I at HWS1 (Figure 5). Based on the field instrumentation results, variations of in situ VSMC and SMS profiles at three different depths with rainfall at the crest and middle of the HWS1 are presented in Figure 9. The sensors provided data at the crest and middle of the slope. It was observed that after January 2020, the highest rainfall occurred in late August 2020. Furthermore, VSMC varied for all three depths at both crest and middle of the slope. On the other hand, SMS showed very little variations at the crest of the slope and some variations in the middle of the slope. The VSMC dropped at the 5 ft (1.5 m) depth in the middle of the slope during fall 2020. The drop in VSMC can be explained by either the soil movement at that depth or a change in vertical hydraulic conductivity. The existence of voids might also result in acute VSMC variations.

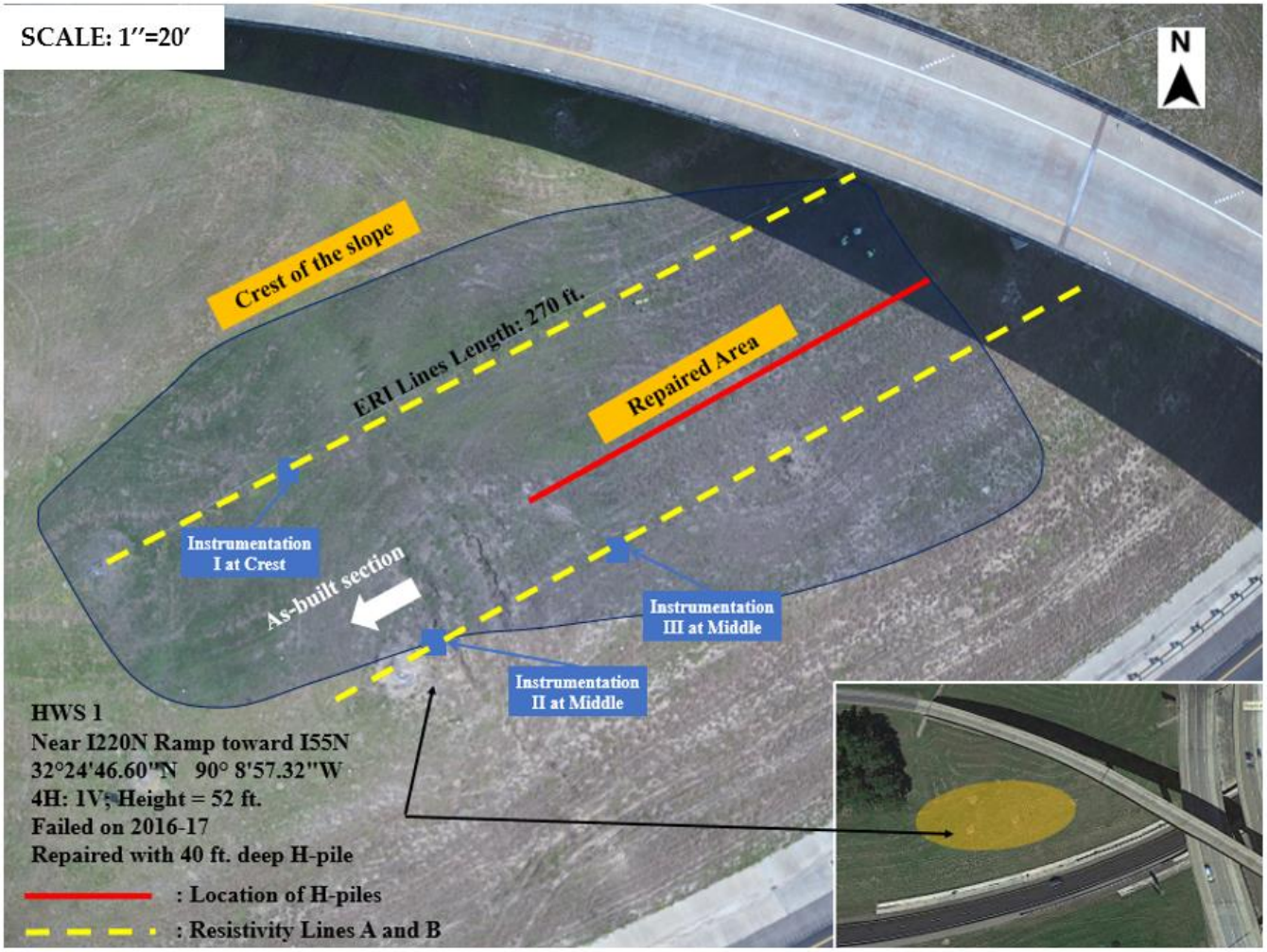

Figure 8. HWS 1 ERI and instrumentation layouts along with its characteristics (drone image-top view) (1′ = 1 ft = 0.305 m).

6.1.2. ERI Layout

The goal of ERI testing was to provide a clear image (data mapping with visualizations) of the subsurface resistivity. SMS and VSMC distribution could be linked to the underlying geological profile. The field ERI inquiry takes data on the apparent resistivity of the soil, which is subsequently analyzed using Advanced Geosciences, Inc.'s EarthImager 2D software (AGI). The apparent resistivity (r) data for this study were gathered during the ERI field investigation using SuperSting R8/IP equipment, downloaded to a computer and analyzed using EarthImager 2D software. Through a mechanism called ERI inversion, the specialist software analyses the field data to create 2D picture parts. The underlying resistivities are mapped using an iterative process based on the least-squares inversion method. The software starts with a projected model with calculated (or expected) resistivities and compares it to the field-measured apparent resistivities. It estimates the root mean squared (RMS) error between measured and expected resistivities and iteratively modifies the predicted (or calculated) resistivities until the RMS error is less than 5% based on the data misfit histogram.

At HWS 1, the ERI test was conducted along a 270 ft (82.3 m) length and the inverted resistivity profiles at Line A and Line B, which correspond to the crest and middle of the slope, respectively, presented in Figure 10. ERI test lines were strategically placed to pass the instrumentation location so that the ERI subsurface imaging results could be compared with the sensor-measured data.

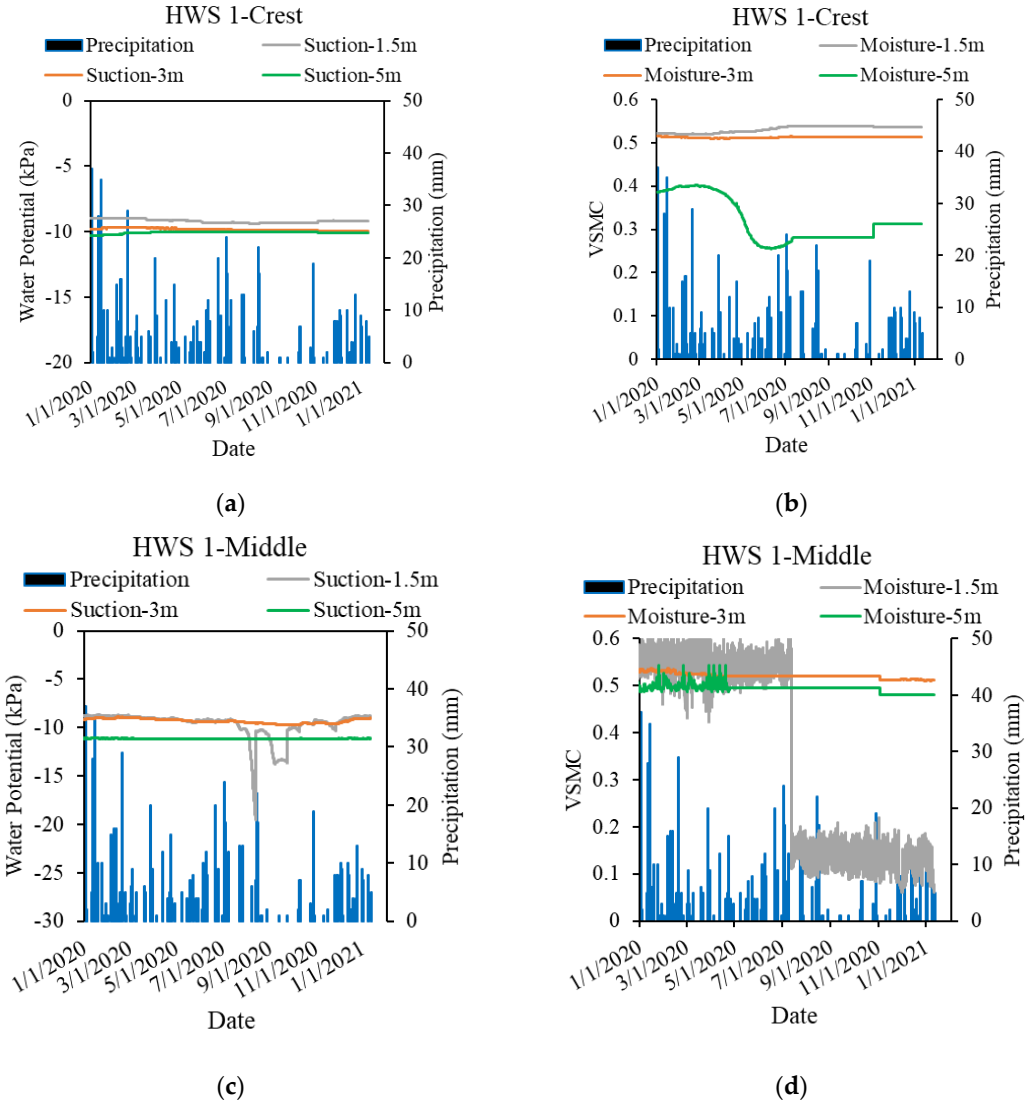

Figure 9. HWS 1 in situ variations with rainfall (**a**) SMS across the crest of the slope (**b**) VSMC across the crest of the slope (**c**) SMS across the middle of the slope (**d**) VSMC across the middle of the slope (1 m = 3.28 ft; 1 mm = 0.039 in; 1 kPa = 20.89 psf).

The field instrumentation provides subsurface data at a confined location (point data), whereas the ERI results provide spatially distributed subsurface information (2D data). Comparing and combining these two results will provide a better understanding of the spatial variations across a wide area and various depths of the HWS. It was observed that the topsoil moved and the surface cracks allowed rainwater to infiltrate and perch in zones up to 30 ft (5 m) depths. It should be noted that the low resistivity values indicate that the soil area was fully saturated. However, the high resistivity values indicated that either the soil area was refilled with another soil type, or the soil had been displaced or the area filled with high stiffened materials.

6.1.3. Data Comparison

The comparison of ERI and field instrumentation results (VSMC and SMS) at the crest and middle of the HWS 1 is presented in Figure 11. It was observed that the soil around the instrumentation location at both crest and middle of the slope was fully saturated, showing low resistivity values. Since the soil has been conditioned in a fully saturated zone for a long time with the existence of daily to weekly rainfall, the SMS was low and constant.

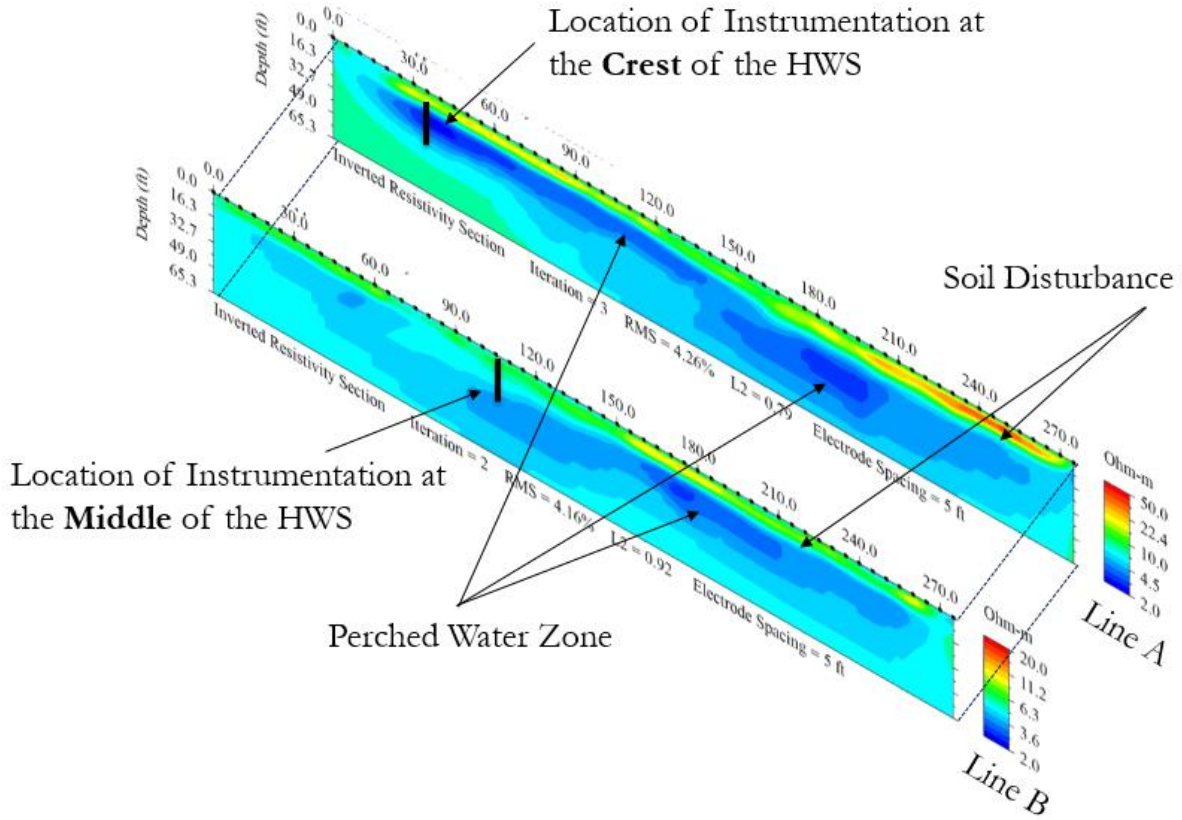

Figure 10. HWS 1, 2D ERI test profile at line A and line B tested on 5 January 2021 (1 ft = 0.3 m).

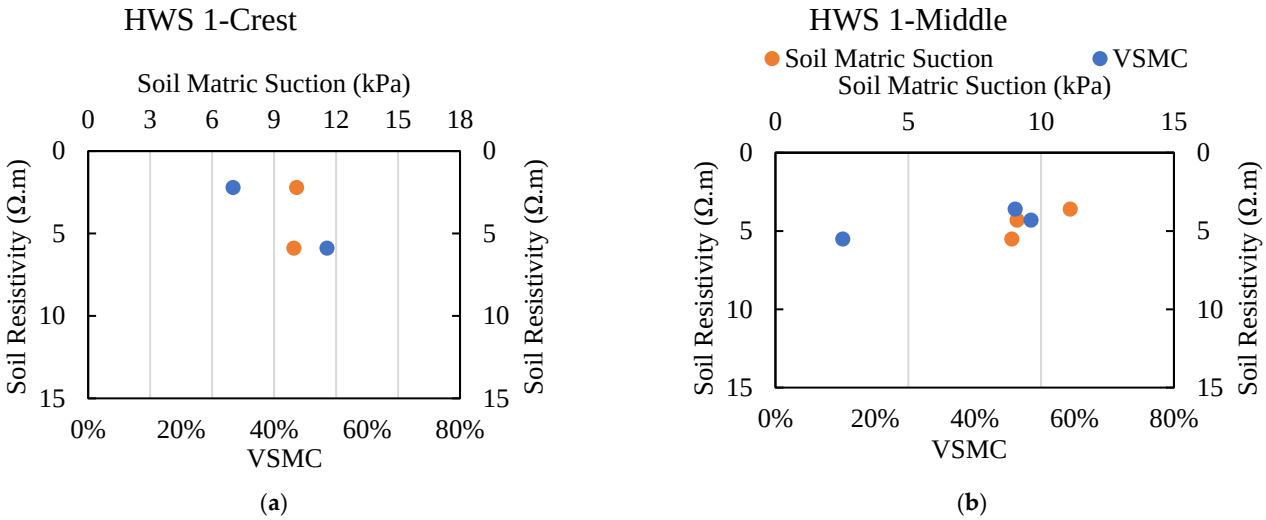

Figure 11. HWS 1 comparison of 2D ERI test profile with field instrumentation (**a**) At crest of the slope (**b**) At middle of the slope (1 m = 3.28 ft.; 1 mm = 0.039 in.; 1 kPa = 20.89 psf).

6.2. HWS 2

The HWS2 is located along I220 N over the ramp from US 80 E and has a reinforced and as-built section, as presented in Figure 12. The failed HWS2 was repaired with a series of deep H-piles. Three 15 ft (5 m) boreholes were drilled and then instrumented at the as-built section at the slope's crest, middle and toe, designated as Instrumentation I, Instrumentation II and Instrumentation III, respectively. The failed and the repaired section of the HWS2 is on the north side and the as-built section is on the south side of the HWS2 as illustrated in Figure 12.

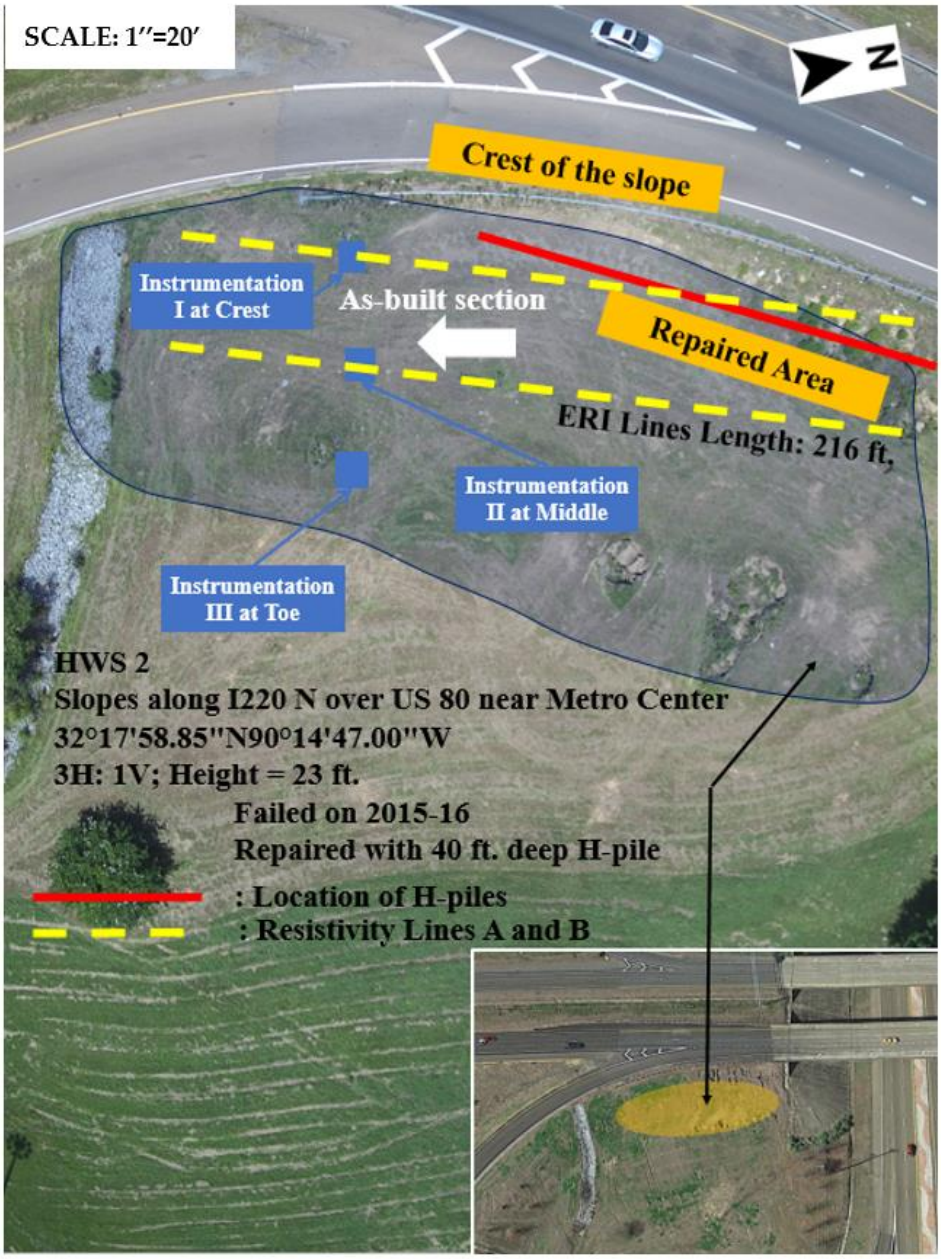

Figure 12. HWS 2 ERI and instrumentation layouts along with its characteristics (drone image-top view) (1′ = 1 ft = 0.305 m).

6.2.1. Instrumentation Layout

In each of the instrumentation locations, at 5 ft (1.5 m), 10 ft (3 m) and 15 ft (5 m) depths, a moisture sensor and a water potential sensor were installed. Additionally, a rain gauge and air temperature sensor were installed at Instrumentation 1 at HWS2 (Figure 5). Variations of in situ matric VSMC and SMS profiles at three different depths with rainfall at both crest and middle of the slope are presented in Figure 13. At Instrumentation I and Instrumentation II, an initial VSMC variation was observed within the first 3 months after instrumentation installation, which can be considered as the adjustment period of the moisture distribution. It should be noted that the SMS at those locations did not present any changes due to the fully saturated condition. In the middle of the slope in Instrumentation II, a variation of the VSMC was observed during the summer 2020 up to late December, indicating rainwater infiltration. The high variation of the VSMC indicated the rainwater infiltration through the surface cracks that were either pre-existing or newly formed during

the dry season. It is likely that a perched water table exists at this slope as it was validated with ERI results and presented in later sections of this study.

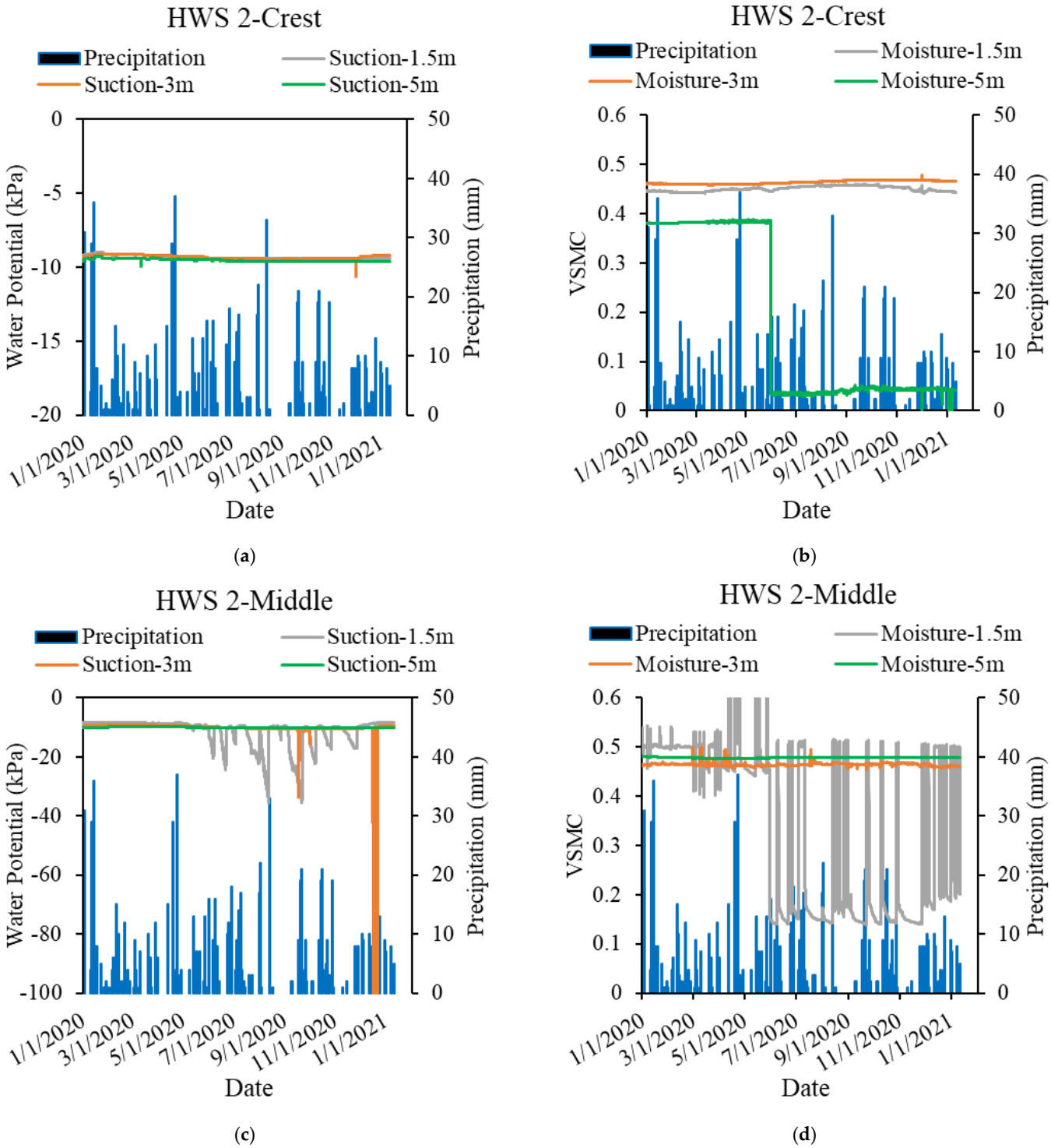

Figure 13. HWS 2 in situ variations with rainfall (**a**) SMS across the crest of the slope (**b**) VSMC across the crest of the slope (**c**) SMS across the middle of the slope (**d**) VSMC across the middle of the slope (1 m = 3.28 ft; 1 mm = 0.039 in; 1 kPa = 20.89 psf).

6.2.2. ERI Layout

The ERI test with two lines was conducted at HWS 2 along a 220 ft (67 m) length at the crest and middle of the slope. The results of the ERI inversion are shown in Figure 14. The ERI images demonstrate that the slope is fully saturated, indicating a high VSMC and very

low SMS. These are the characteristics of a soft and low soil strength, which is prone to show signs of movement in the near future. There are perched water zones directly below the unsaturated soil zones in the center of the slope (Figure 14). The high resistivity values indicated the soil had been displaced due to the slope movement.

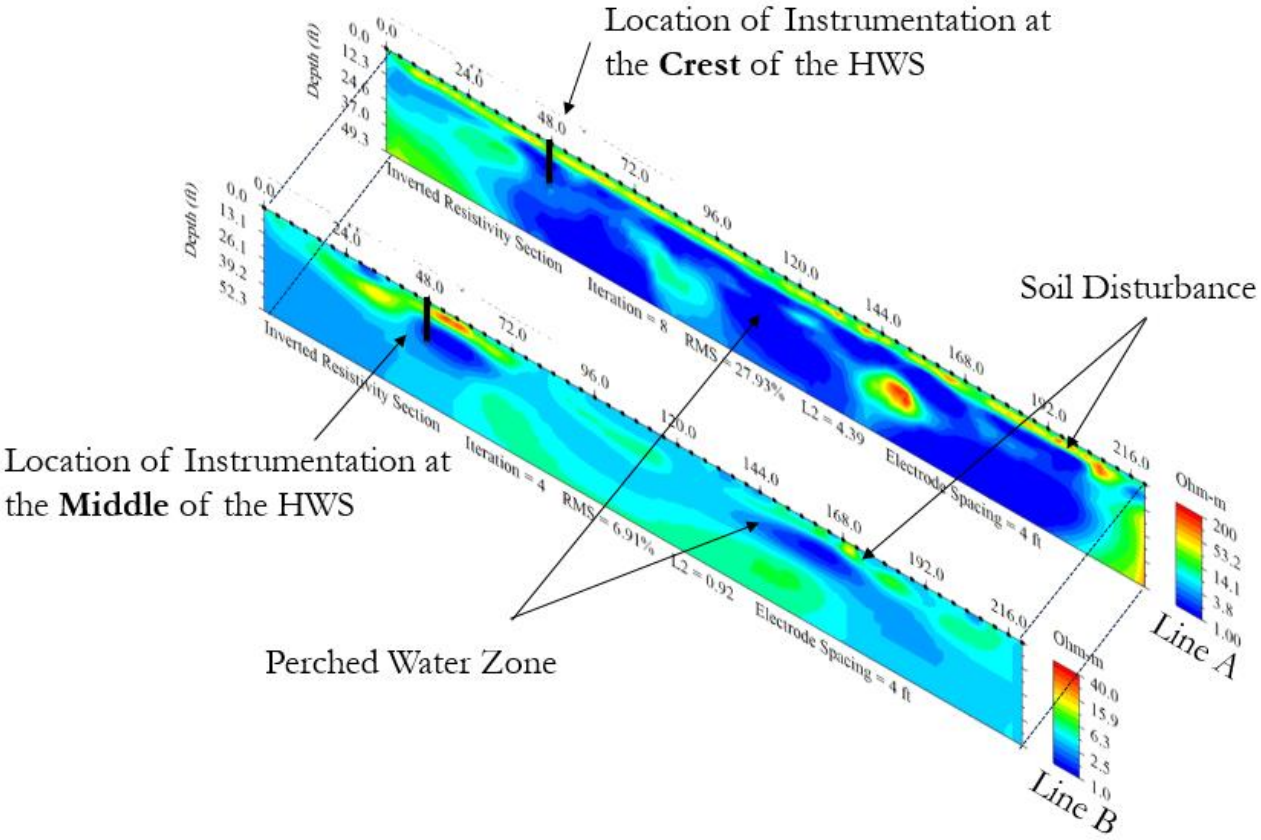

Figure 14. HWS 2, 2D ERI test profile at line A and at line B tested on 7 January 2021 (1 ft = 0.3 m).

6.2.3. Data Comparison

The VSMC and SMS from field instrumentation were compared numerically with ERI test results at both crest and middle of the HWS2, as depicted in Figure 15. It was observed that at the middle of the slope, the inverse relationship between resistivity and low VSMC and relatively high SMS does not exist due to the soil's high degree of saturation. Similar findings were found in this study for other HWS at different depths and locations as well. It was also observed that with a very low VSMC, the SMS has a relatively higher SMS value, which did not impact the resistivity values. Based on ERI results, it was observed that the HWS was fully saturated at 5 ft (1.5 m) depth at the instrumentation location.

6.3. HWS 3

HWS3 is located at I20 E exit toward Terry Road and has reinforced and as-built sections, as presented in Figure 16. The failed HWS3 was repaired with a series of deep H-piles. Two 15 ft (5 m) boreholes were drilled and then instrumented at the repaired sections. These two boreholes were designated as Instrumentation I and Instrumentation II (Figure 16). The third 15 ft (5 m) deep borehole was drilled close to the as-built section and then instrumented; this instrumentation location was designated as Instrumentation III. Instrumentation I is at the crest, whereas Instrumentation II and Instrumentation III are at the middle of the slope.

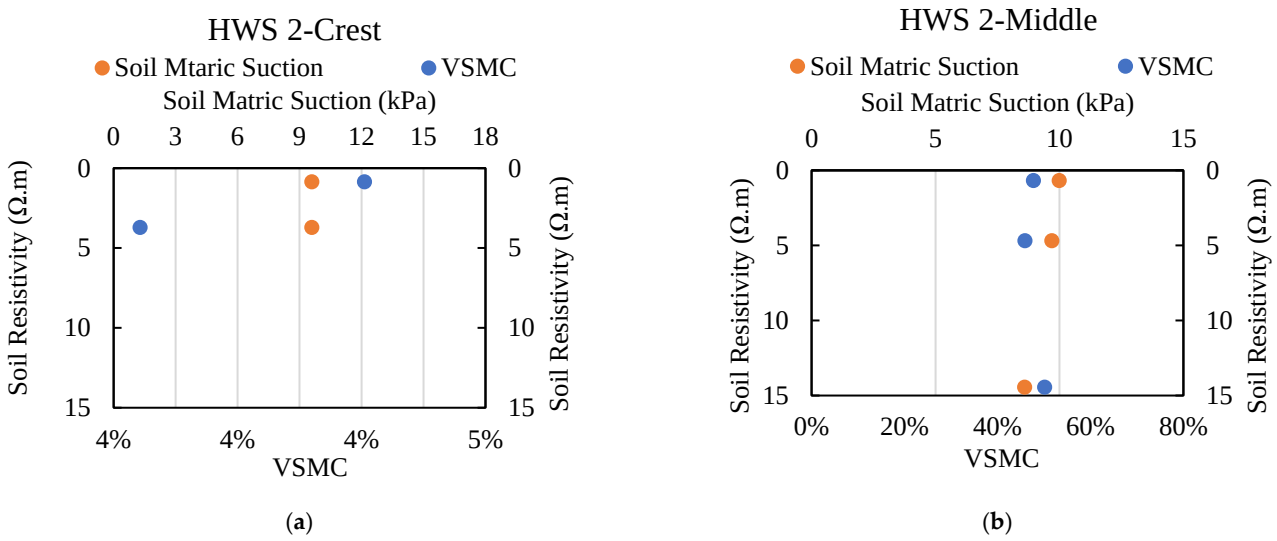

Figure 15. HWS 2 comparison of 2D ERI test profile with field instrumentation (**a**) At crest of the slope (**b**) At middle of the slope (1 m = 3.28 ft; 1 mm = 0.039 in; 1 kPa = 20.89 psf).

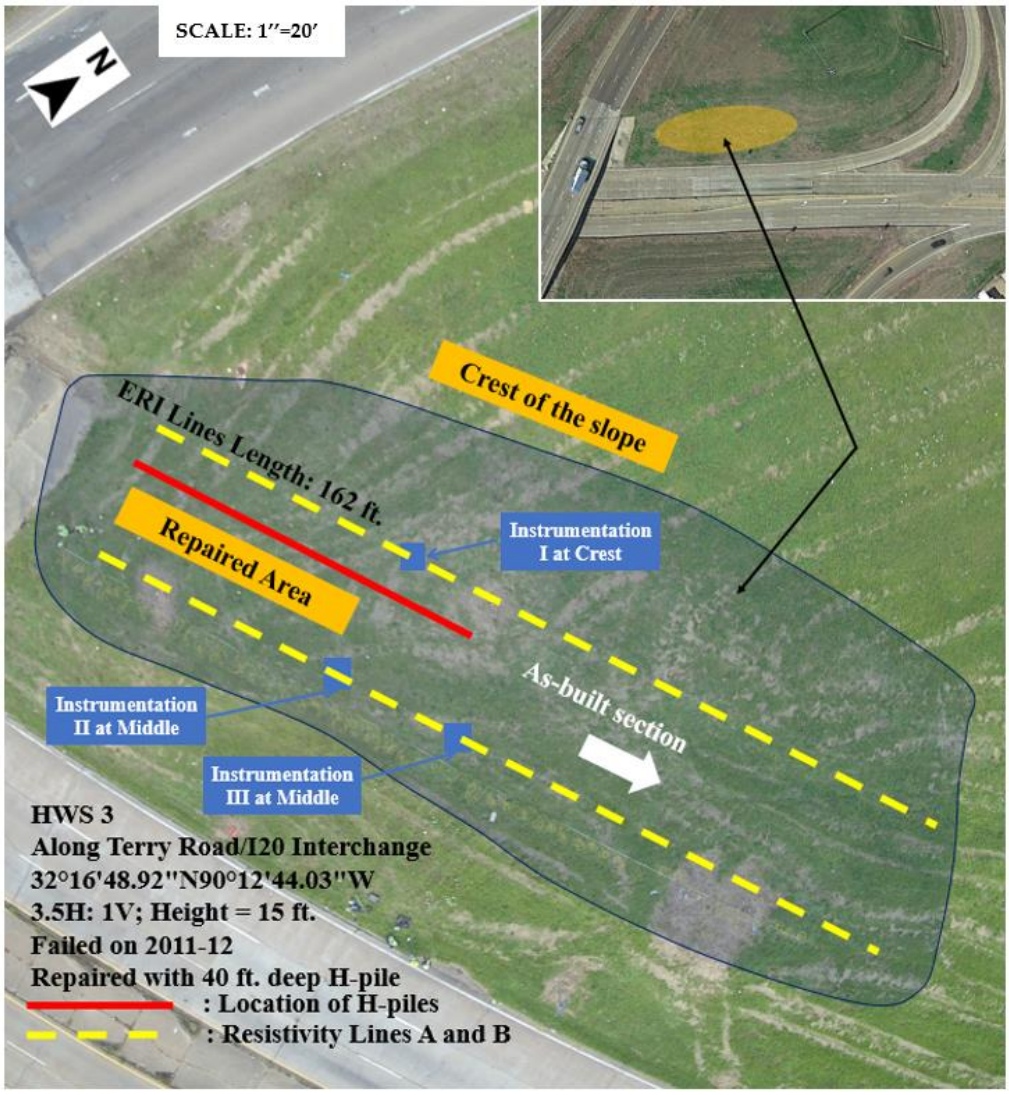

Figure 16. HWS 3 ERI and instrumentation layouts along with its characteristics (drone image-top view) (1′ = 1 ft = 0.305 m).

6.3.1. Instrumentation Layout

In each of the instrumentation locations, at 5 ft (1.5 m), 10 ft (3 m) and 15 ft (5 m) depths, a moisture sensor and a water potential sensor were installed. Additionally, a rain gauge and air temperature sensor were installed at Instrumentation I at HWS3 (Figure 5). Variations of in situ VSMC and SMS profiles with rainfall and depth at the crest and middle of the HWS3 are presented in Figure 17. The SMS sensor recorded a high number for around three months and then reached an equilibrium condition with minor variations until the end of the monitoring period. The VSMC showed high variations at different depths and at different locations due to infiltration. The constant VSMC at the slope is highly possible when there is no moisture variation or when the soil is in a fully saturated condition. The low SMS values signify that the soil is practically close to a fully saturated condition. This is likely possible when there is a formation of perched water conditions at the slope. It should be noted that the as-built section of HWS3 has experienced shallow movement starting in January 2019 [25]. In addition, it is evident from the instrumentation results that there is a presence of perched water conditions at the slope. Therefore, the movement at the as-built section of the slope is taking place due to the formation of perched water with the top part of the slope.

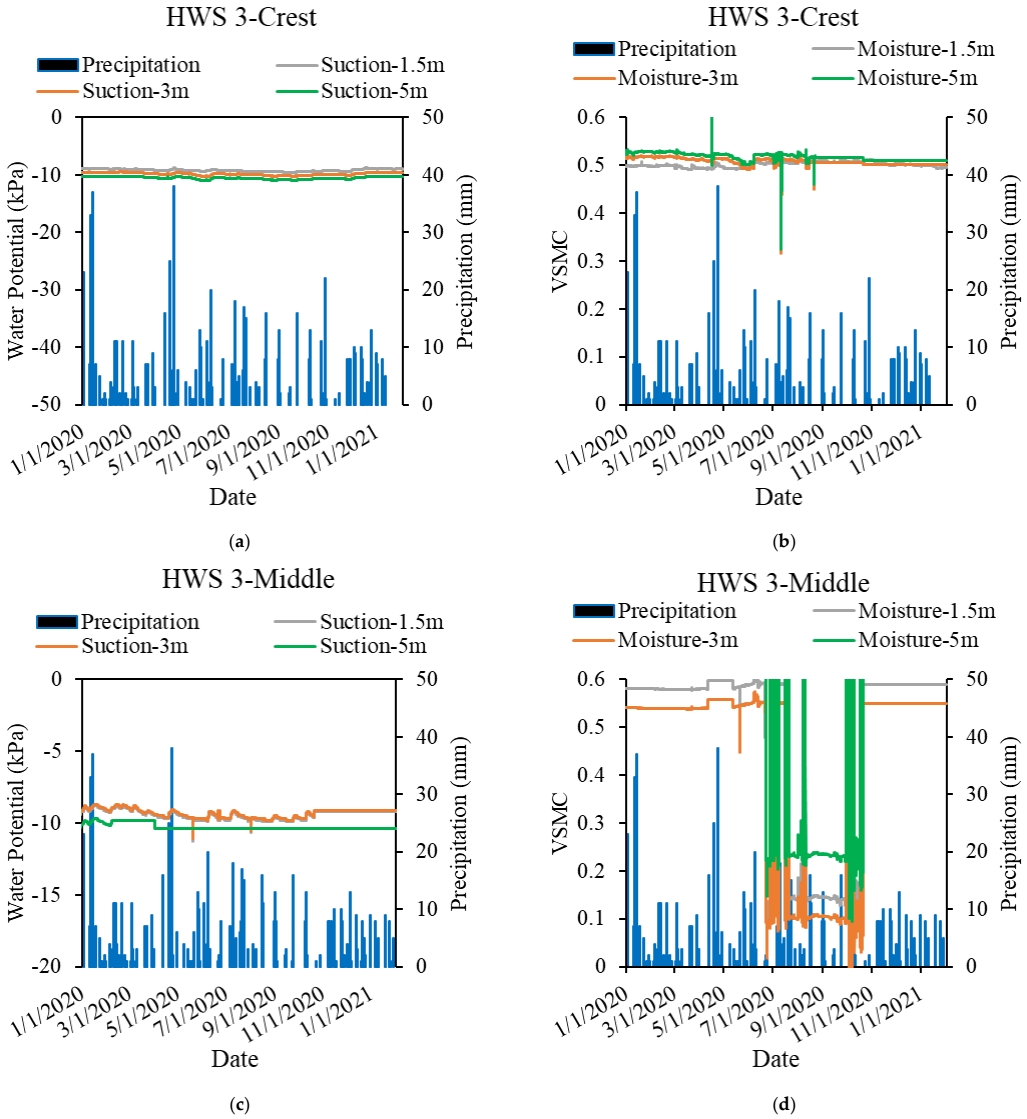

Figure 17. HWS 3 in situ variations with rainfall (**a**) SMS across the crest of the slope (**b**) VSMC across the crest of the slope (**c**) SMS across the middle of the slope (**d**) VSMC across the middle of the slope (1 m = 3.28 ft; 1 mm = 0.039 in; 1 kPa = 20.89 psf).

6.3.2. ERI Layout

Figure 18 presents the ERI test along a 165 ft (50.2 m) length of the crest and middle (lines A and B) of the HWS3. The ERI inversion images show high resistivity at the top-soil layers due to the different soil types (low plastic soil) as it was used during the reconstruction of the failed slope. The filled soil type had higher resistance than the previously existing soil and in this case, the high resistance was not due to soil body displacement. It is observed that the location field instrumentation is located in the fully saturated zone. The perched water zones were located at deeper soil layers along the slope.

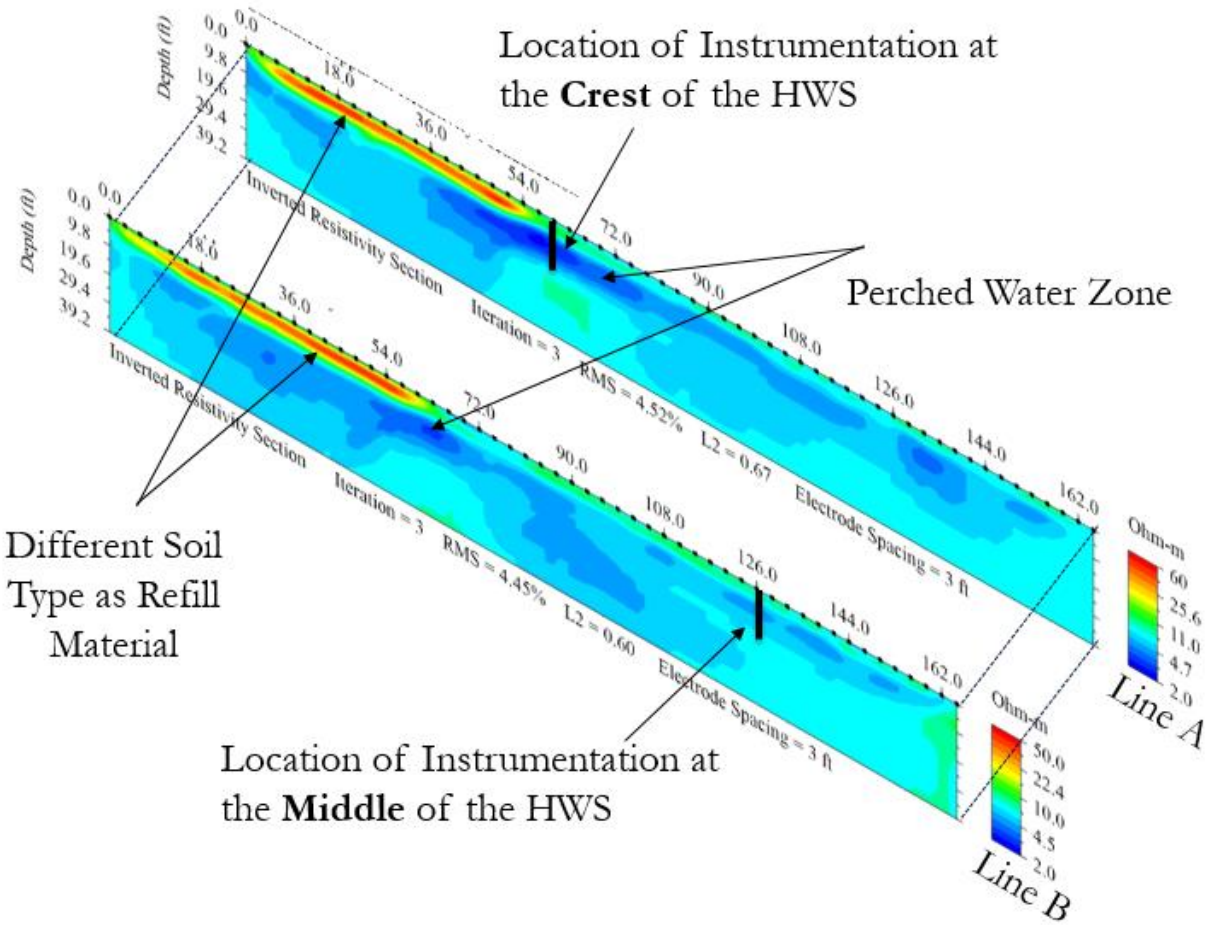

Figure 18. HWS 3, 2D ERI test profile at line A and at line B tested on 9 January 2021 (1 ft = 0.3 m).

6.3.3. Data Comparison

Figure 19 shows the ERI and field instrumentation results comparison. It is observed that the values of the VSMC and SMS at the depth and location of the instrumentation did not have a significant impact on the soil resistivity variation. High VSMC and low SMS observations at the crest and middle of HWS3 coincided with low soil resistivity values, which was a common finding at all the slopes in this study.

6.4. HWS 4

The HWS4 is located along I20 E near Highland drive, as presented in Figure 20. Three 15 ft (5 m) boreholes were drilled and then instrumented at the crest, middle and toe of the HWS, which were designated as Instrumentation I, Instrumentation II and Instrumentation III, respectively. The HWS showed signs of soil body movements from the project starting the day of monitoring. Over time, multiple voids have developed on the slope, which has impacted the permeability of the soil and associated flow characteristics.

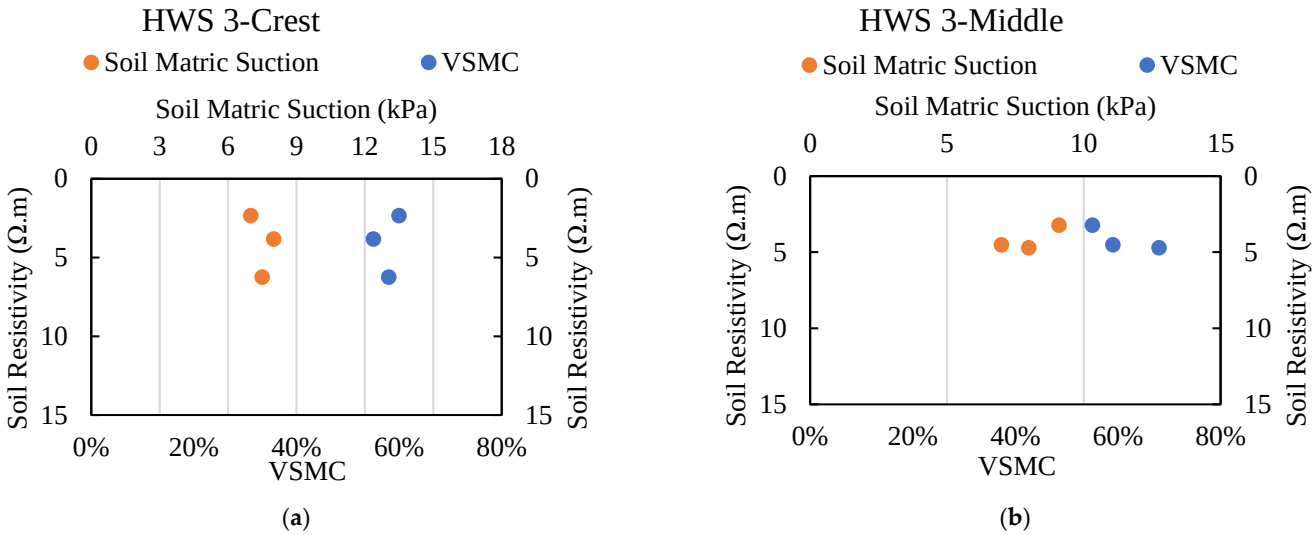

Figure 19. HWS 3 comparison of 2D ERI test profile with field instrumentation (**a**) At crest of the slope (**b**) At middle of the slope (1 m = 3.28 ft; 1 mm = 0.039 in; 1 kPa = 20.89 psf).

Figure 20. HWS 4 ERI and instrumentation layouts along with its characteristics (drone image-top view) (1′ = 1 ft = 0.305 m).

6.4.1. Instrumentation Layout

The instrumentation types, quantity and arrangement were similar to the previously mentioned HWS (Figure 5). Figure 21 shows the change of in situ VSMC and SMS profiles

at three different depths and different locations with rainfall. Based on the field monitoring results, it was observed that due to the existence of voids at the field, at a shallower depth in the slope soil body, a high variation of VSMC and SMS occurred. The formation and development of perched water zones are observed at deeper soil layers, which impact the variation of both VSMC and SMS.

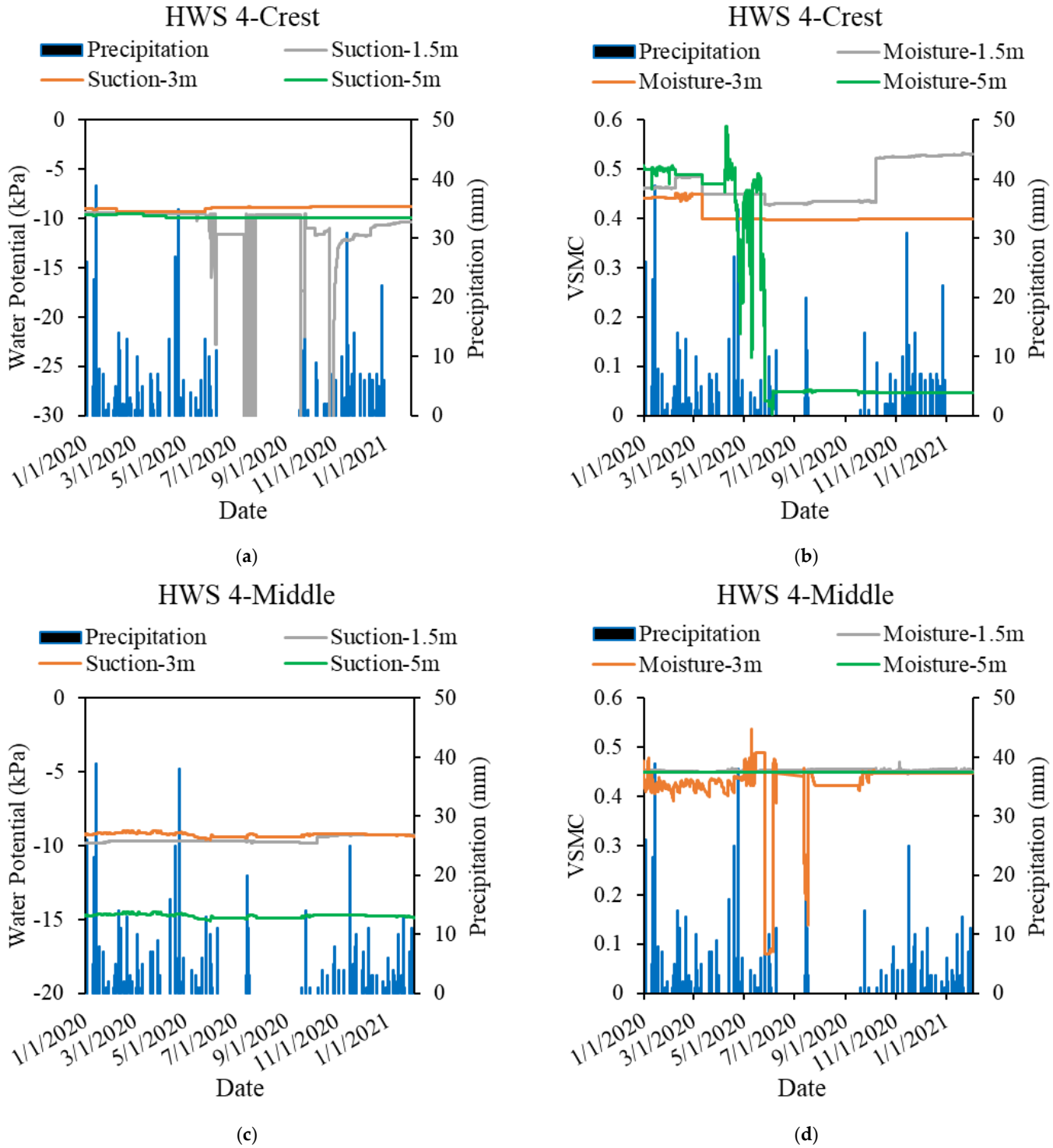

Figure 21. HWS 4 in situ variations with rainfall (**a**) SMS across the crest of the slope (**b**) VSMC across the crest of the slope (**c**) SMS across the middle of the slope (**d**) VSMC across the middle of the slope (1 m = 3.28 ft; 1 mm = 0.039 in; 1 kPa = 20.89 psf).

6.4.2. ERI Layout

The ERI test was conducted at HWS 4 for a horizontal length of 162 ft (49.3 m) between the crest and the middle of the HWS (Lines A and B). The results of the ERI inversion profile are shown in Figure 22. The ERI results show that extremely high resistivity zones were discovered at both the crest and middle of the HWS. High resistive areas were observed at the surficial levels in the middle, mostly due to the existence of voids. At deeper levels, perched water zone development is noticeably indicated in blue on ERI results in Figure 22.

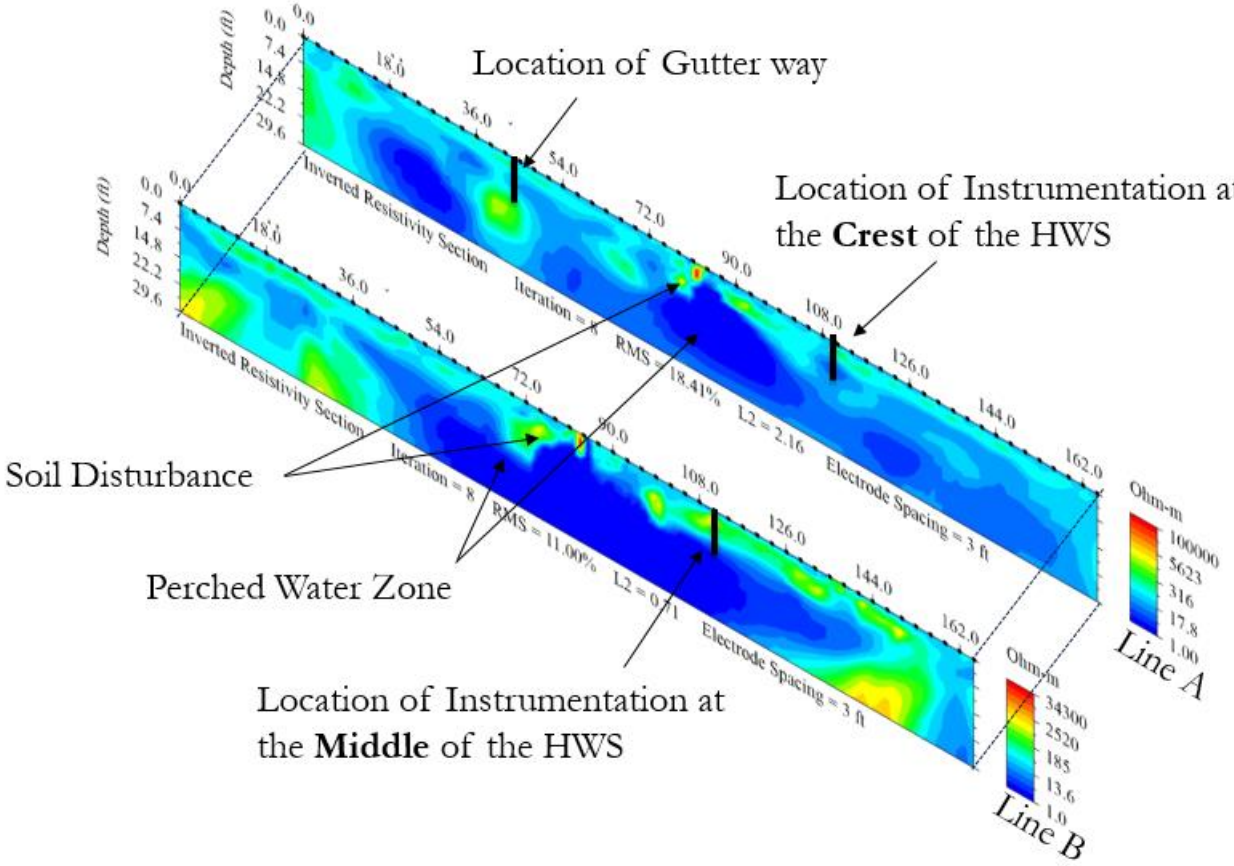

Figure 22. HWS 4, 2D ERI test profile at line A and at line B tested on 11 January 2021 (1 ft = 0.3 m).

6.4.3. Data Comparison

The ERI, VSMC and SMS results at instrumentation locations were compared and are presented in Figure 23. Similar to other HWS studied in this paper, it was observed that the instrumentations located at the top of the perched water zone resulted in low values of soil resistivity and SMS with high VSMC.

6.5. HWS 5

HWS5 is located along I55 South and Sowell Road and has reinforced and as-built sections, as presented in Figure 24. The failed area was repaired with a series of deep H-piles. Two 15 ft (5 m) boreholes were drilled at the as-built sections for instrumentation. These two boreholes were designated as Instrumentation I and Instrumentation II. A third 15 ft (5 m) deep borehole was drilled and then instrumented close to the reinforced section, which was designated as Instrumentation III. Instrumentation I was located at the crest, whereas Instrumentation II and Instrumentation III were located in the middle of the slope.

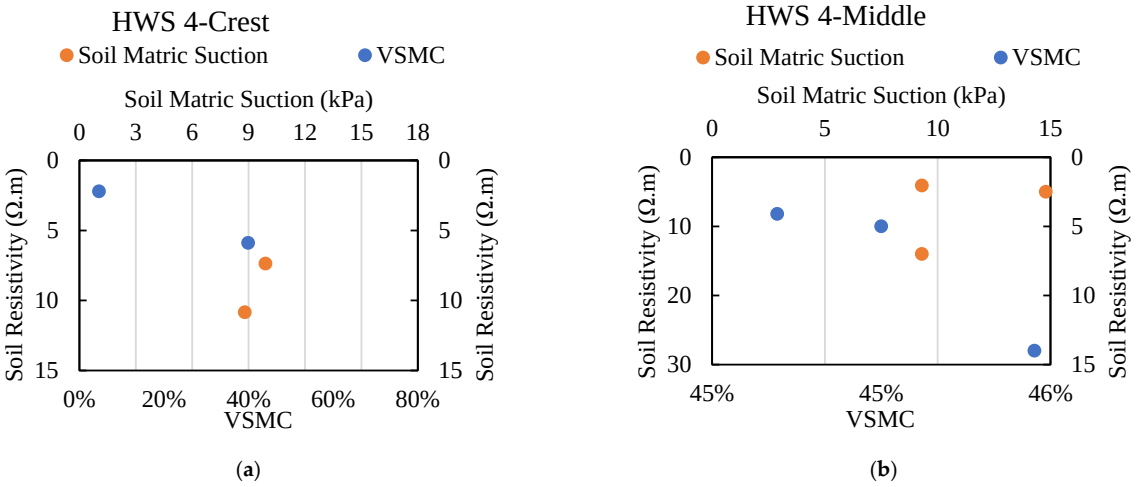

Figure 23. HWS 4 comparison of 2D ERI test profile with field instrumentation (**a**) At crest of the slope (**b**) At middle of the slope (1 m = 3.28 ft; 1 mm = 0.039 in; 1 kPa = 20.89 psf).

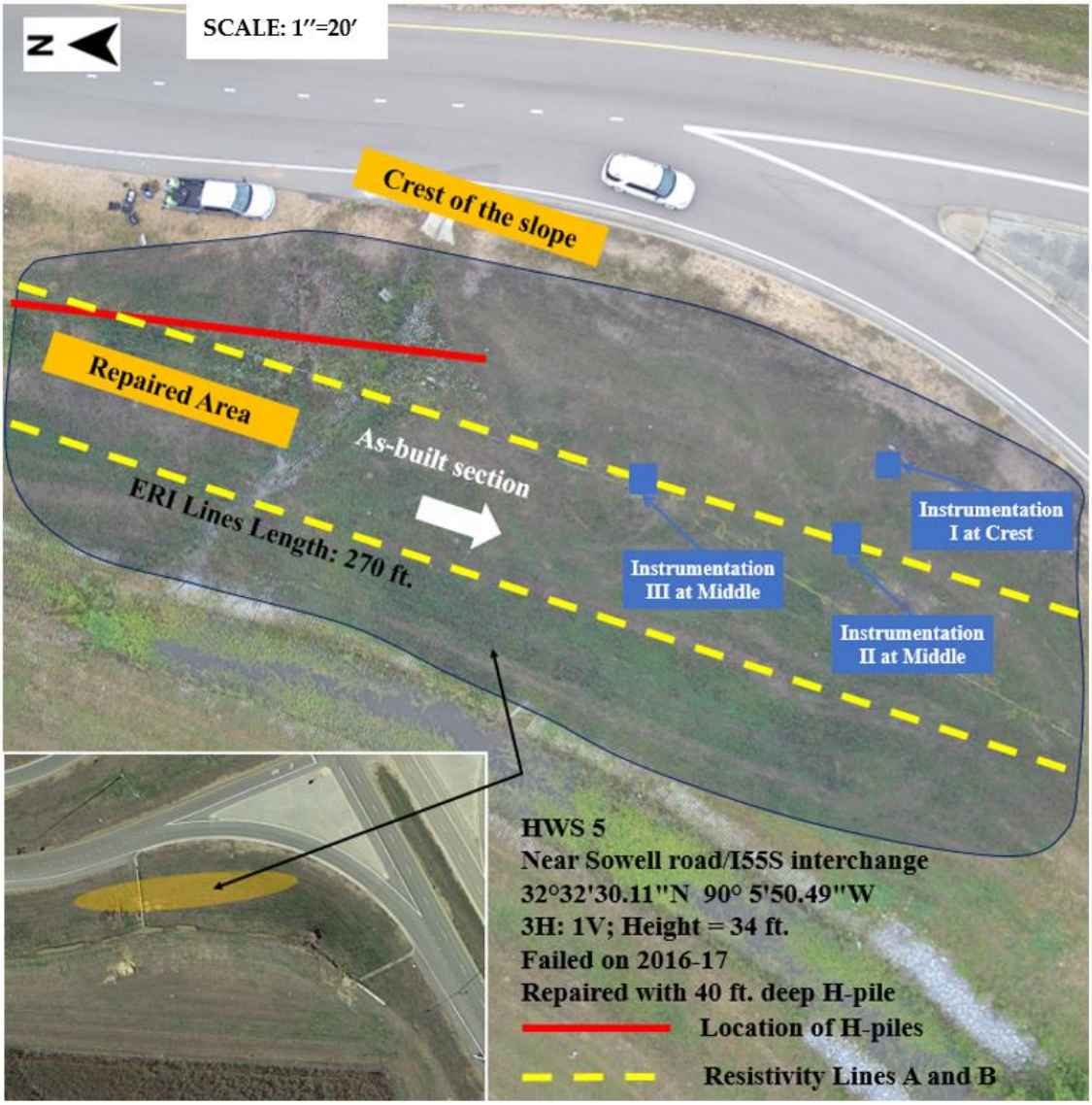

Figure 24. HWS 5 ERI and instrumentation layouts along with its characteristics (drone image-top view) (1′ = 1 ft = 0.305 m).

6.5.1. Instrumentation Layout

The sensor selection, arrangement and layouts are the same as the previously mentioned HWS instrumentation plans (Figure 5). Figure 25 presents the change in VSMC and SMS profiles with daily rainfall recordings at the crest and middle of the HWS and at different depths. Specifically, the results are recorded at three instrumentation locations (I, II and III) and at three different depths 5 ft (1.5 m), 10 ft (3 m) and 15 ft (5 m). Since the slope has experienced a failure during the early part of this study, special emphasis was given to the rainfall before the failure. Based on the instrumentation results, the SMS of the slopes remains constant after the preliminary 2–3 months of the observation period. In addition, the lower SMS value was present at the top part of the slope, which signifies low shear strength and high VSMC. The slope has experienced a significant VSMC variation during the dry period, mostly at 5 ft (1.5 m) and 10 ft (3 m) depths. This significant variation of VSMC indicated that the slope had shrinkage cracks during the summer, creating a preferential path for rainwater infiltration.

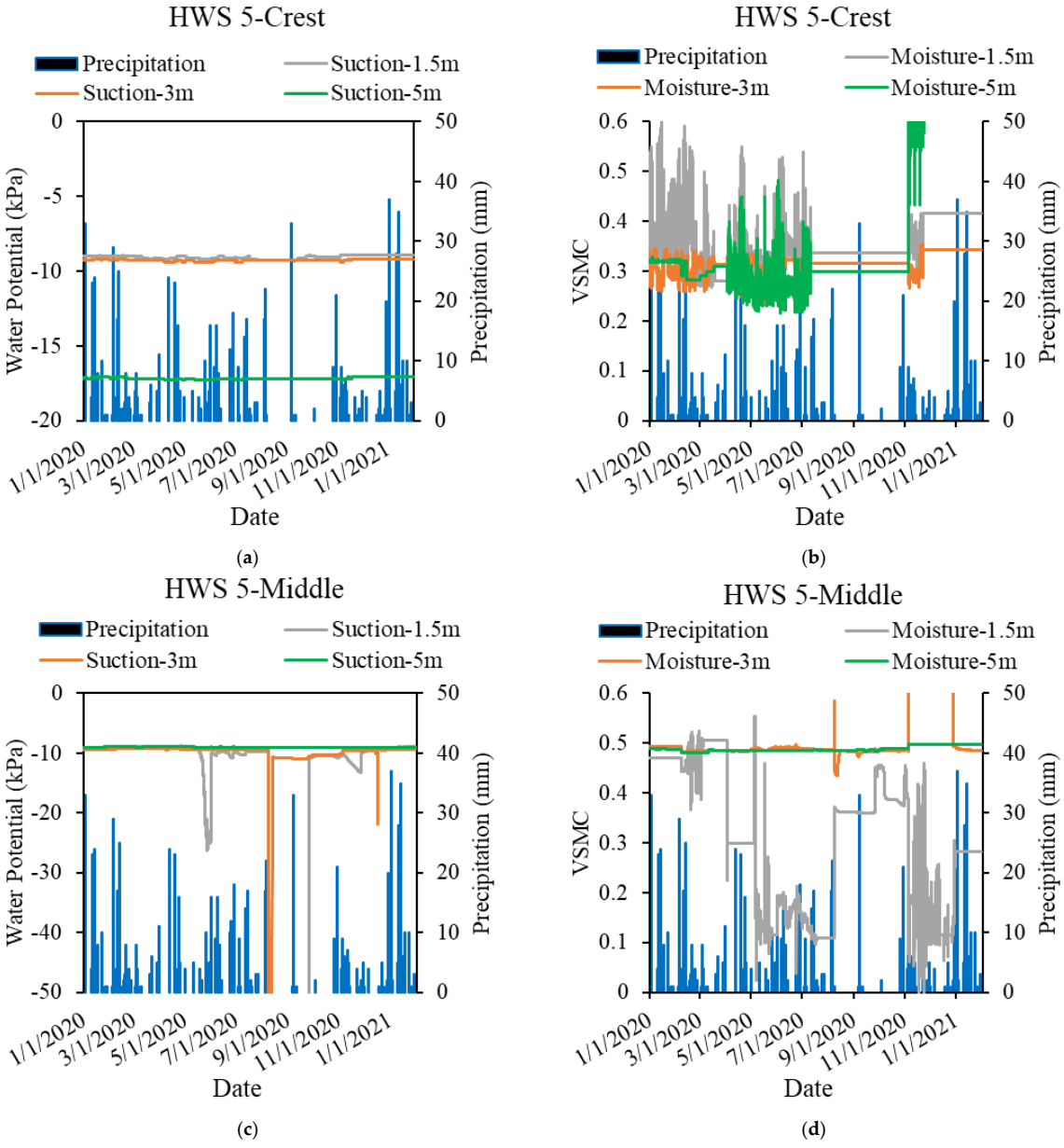

Figure 25. HWS 5 in situ variations with rainfall (**a**) SMS across the crest of the slope (**b**) VSMC across the crest of the slope (**c**) SMS across the middle of the slope (**d**) VSMC across the middle of the slope (1 m = 3.28 ft; 1 mm = 0.039 in; 1 kPa = 20.89 psf).

6.5.2. ERI Layout

Figure 26 presents the ERI inversion profile results for both line A and line B. The formation of the perched water zone can be noticed in deeper soil layers and along the slope. Some minor soil displacements occurred at the slope soil surficial layers. The developed perched water zone under the location of the gutter way indicated that part of the rainwater infiltrated and trapped in deeper soil layers, which are high plastic clay soils. Comparing ERI results with the field instrumentation results, it is observed that both VSMC and SMS showed higher variations along depths. It was observed that the location of the instrumentation in the middle of the slope is not close to the perched water zone, unlike the other slopes in this study.

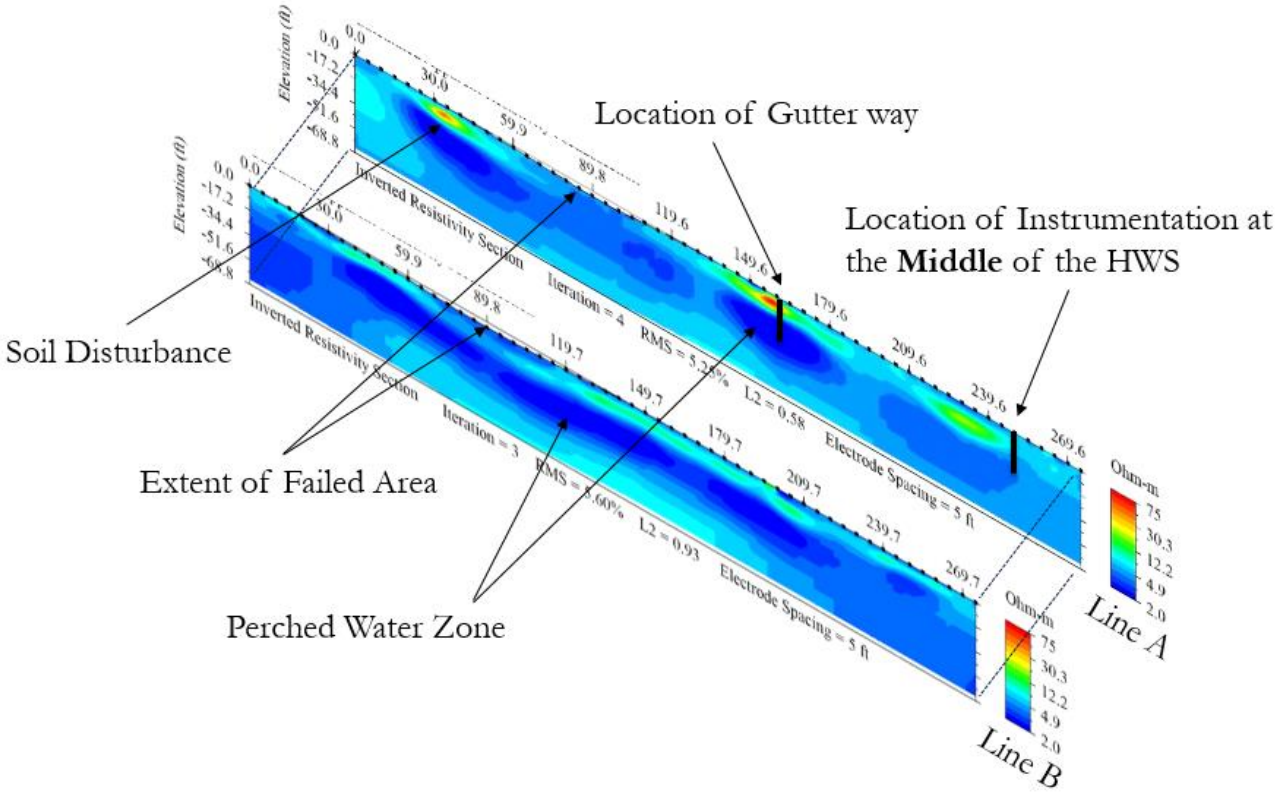

Figure 26. HWS 5, 2D ERI test profile at line A and at line B tested on 13 January 2021 (1 ft = 0.3 m).

6.5.3. Data Comparison

The ERI test results comparisons with VSMC and SMS at different locations are presented in Figure 27. The expected relationship between resistivity, VSMC and SMS is such that lower resistivity values correspond with higher VSMC and lower SMS. However, in most of the HWS in this study, the expected relationship between ERI, VSMC and SMS did not exist. Resistivity and SMS values were observed to be low for HWS5, and the VSMC did not play a role in impacting these values. This is because the HWS soil body was either partially saturated or fully saturated for most of the year due to recurrent rainfall events. ERI results show low resistivity values all over the HWS subsurface, indicating the likelihood of perched water zones all over the subsurface.

6.6. HWS 6

HWS 6 is located along I20 E near McRaven road. The HWS6 descriptive illustrations are presented in Figure 28. The HWS has shown signs of movement. Three 15 ft (5 m) boreholes were drilled and then instrumented at the crest, middle and toe of the slope. In Figure 28, the three instrumentation locations are designated as Instrumentation I, Instrumentation II and Instrumentation III.

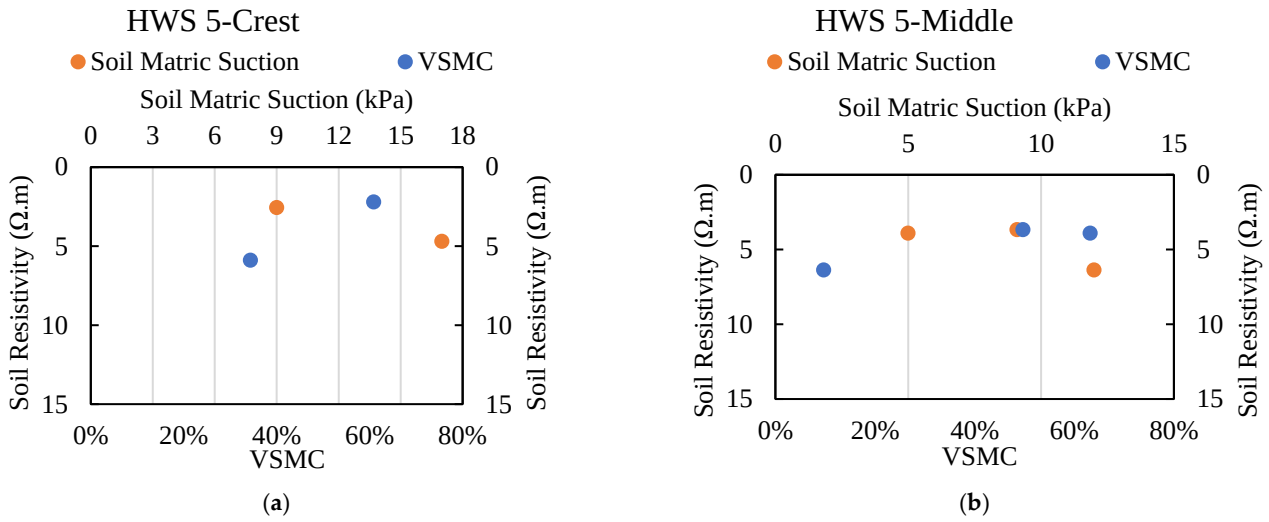

Figure 27. HWS 5 comparison of 2D ERI test profile with field instrumentation (**a**) At crest of the slope (**b**) At middle of the slope (1 m = 3.28 ft; 1 mm = 0.039 in; 1 kPa = 20.89 psf).

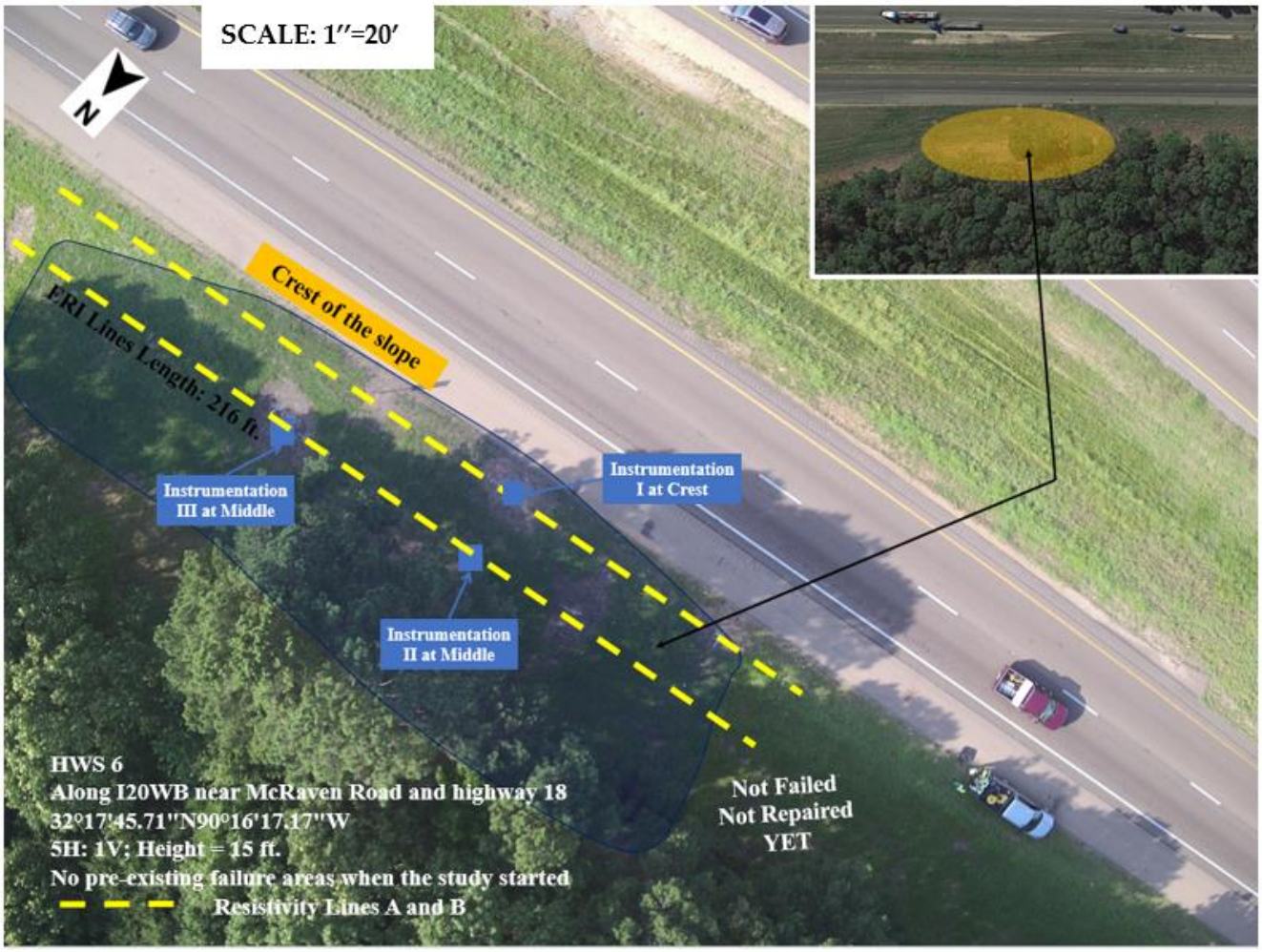

Figure 28. HWS 6 ERI and instrumentation layouts along with its characteristics (drone image-top view) (1′ = 1 ft = 0.305 m).

6.6.1. Instrumentation Layout

Similar to the previously mentioned HWS, in each of the instrumentation locations, at 5 ft (1.5 m), 10 ft (3 m) and 15 ft (5 m) depths on HWS6, a moisture sensor and a water potential sensor were installed. Additionally, a rain gauge and air temperature sensorwere installed at Instrumentation 1 at slope 6 (Figure 5). Variations of in situ VSMC and SMS profiles at 5 ft (1.5 m), 10 ft (3 m) and 15 ft (5 m) depths with rainfall at the three instrumentation locations are presented in Figure 29. Based on the field monitoring results, the SMS has a high number for around three months and then reached an equilibrium condition. SMS values observed were low and did not change much over the course of the monitoring period, similar to other HWS. VSMC also showed low variations throughout the monitoring period, except during late 2020 and early 2021. As observed from the ERI results shown in Figure 30, the soil is likely to be close to a fully saturated condition. Therefore, VSMC and SMS did not show many variations.

The SMS varied with time only at the 5 ft (1.5 m) depth of all the HWS except for HWS 5, where significant SMS variation was observed at the middle of the slope as well (Figure 24). Following a brief decline in SMS potential at shallow depths, SMS values rebounded during the summer. This correlated to a decrease in the VSMC level at 5 ft (1.5 m) depth during the summer months because of decreased rainfall and increased temperatures. This suggests that in the slope soil layers (Yazoo clay) upper unsaturated zone, an inverse relationship exists between VSMC and SMS. However, there were no significant changes in SMS or VSMC associated with rainfall at depths of around 10 ft (3 m) and 15 ft (5 m). As a result, it can be inferred that the soil layers are completely saturated beyond the 10 ft (3 m) depth. Additionally, consistent with previous research on Yazoo clay HWS [25], rainfall water is retained in perched water zones at the shallow levels of the high-plastic Yazoo clay HWS. Furthermore, water infiltration to deeper levels takes a significant period of time, leading to trapped perched water zones.

6.6.2. ERI Layout

Figure 30 presents the ERI test along a 217 ft (66.1 m) length of the crest and middle (lines A and B) of the HWS6. The ERI inversion images reveal a relatively high resistivity at the top-soil layers due to the soil disturbance. It is observed that the location of field instrumentations located at the fully saturated zones with the developed perched water zones directly impacted the low variations in both VSMC and SMS in that specific area. Unlike the middle of the slope (ERI line B), the development of perched water zones was observed to be located almost in all deeper soil layers along with line A at the slope.

Considering the ERI results of all six referenced HWS, despite the soil disturbance at surficial layers due to the slope soil body and different fill materials, which caused the resistivity values to increase, the upper slope soil layers had higher resistivity values and the deeper slope soil layers had lower resistivity values. Khan et al. [3] showed that the soil layers on most of the referenced slopes were composed of weathered Yazoo clay to a depth of around 30 feet (9 m) and unweathered Yazoo clay beyond 30 ft (9 m). It is observed that the upper layers are softer than the deeper layers consisting of Yazoo clay soils.

6.6.3. Data Comparison

Figure 31 shows the ERI and field instrumentation results comparison for HWS6. It is observed that the values of the VSMC and SMS at the depth and location of the instrumentation did not have a significant impact on the soil resistivity variations. Due to the formation of perched water zone, recurrent rainfall events, soil type characteristics (high plastic clay soil) and the existence of shrinkage cracks, the soil has a low resistivity, relatively high VSMC and low SMS, which could be repeatedly observed in all studied HWSs.

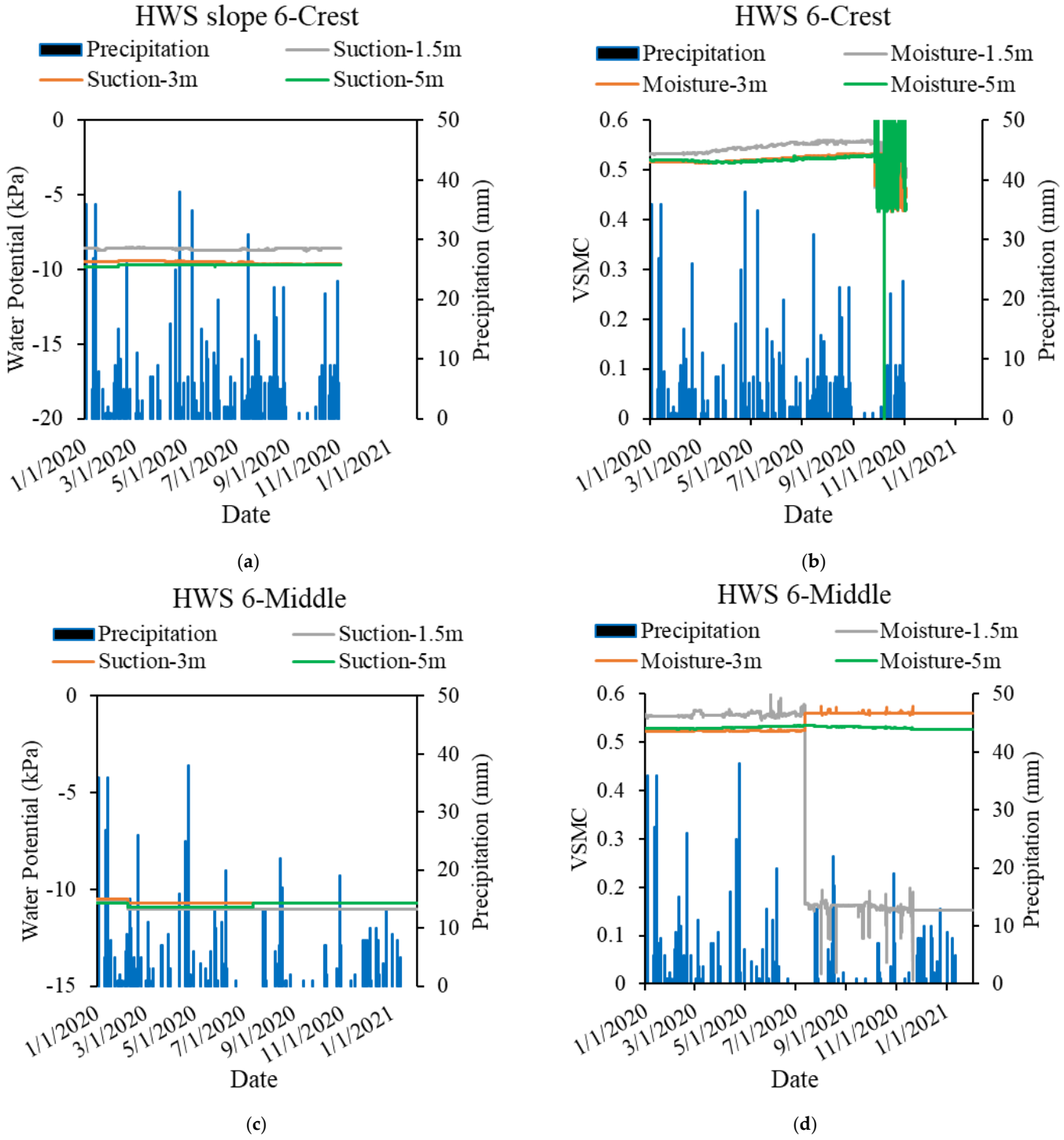

Figure 29. HWS 6 in situ variations with rainfall (**a**) SMS across the crest of the slope (**b**) VSMC across the crest of the slope (**c**) SMS across the middle of the slope (**d**) VSMC across the middle of the slope (1 m = 3.28 ft; 1 mm = 0.039 in; 1 kPa = 20.89 psf).

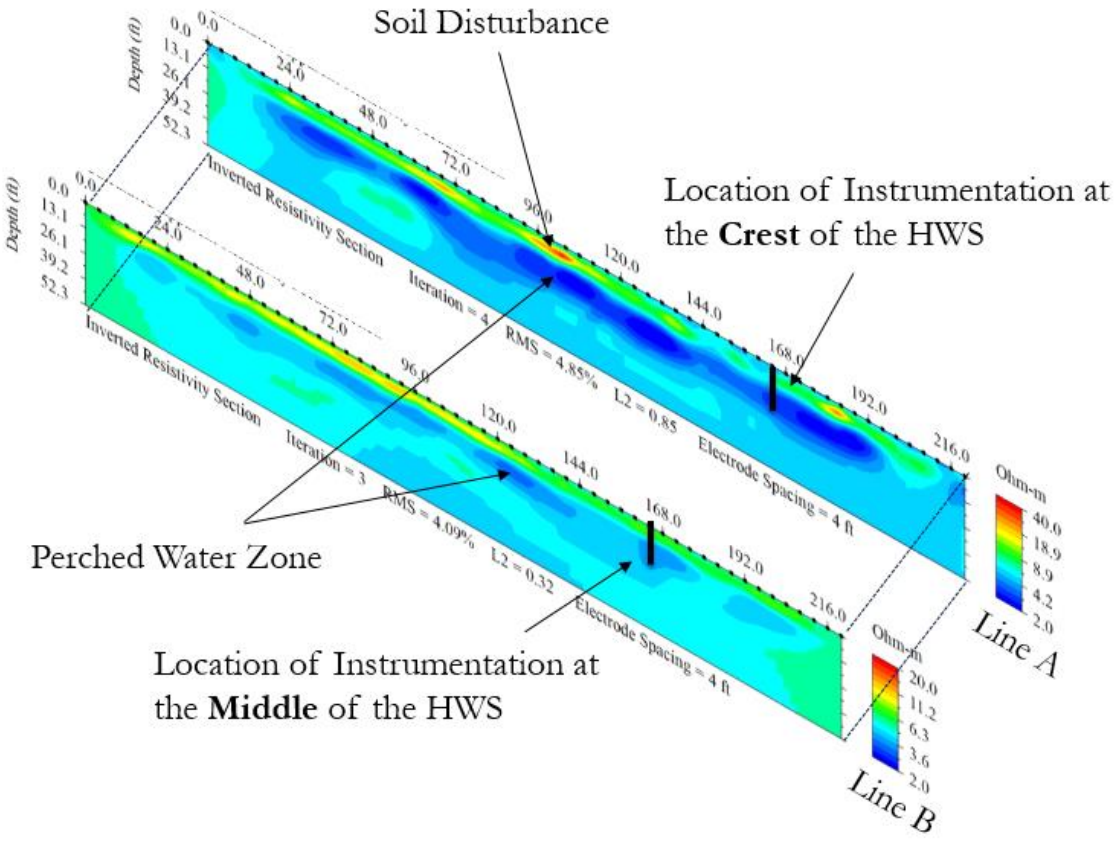

Figure 30. HWS 6, 2D ERI test profile at line A and at line B tested on 15 January 2021 (1 ft = 0.3 m).

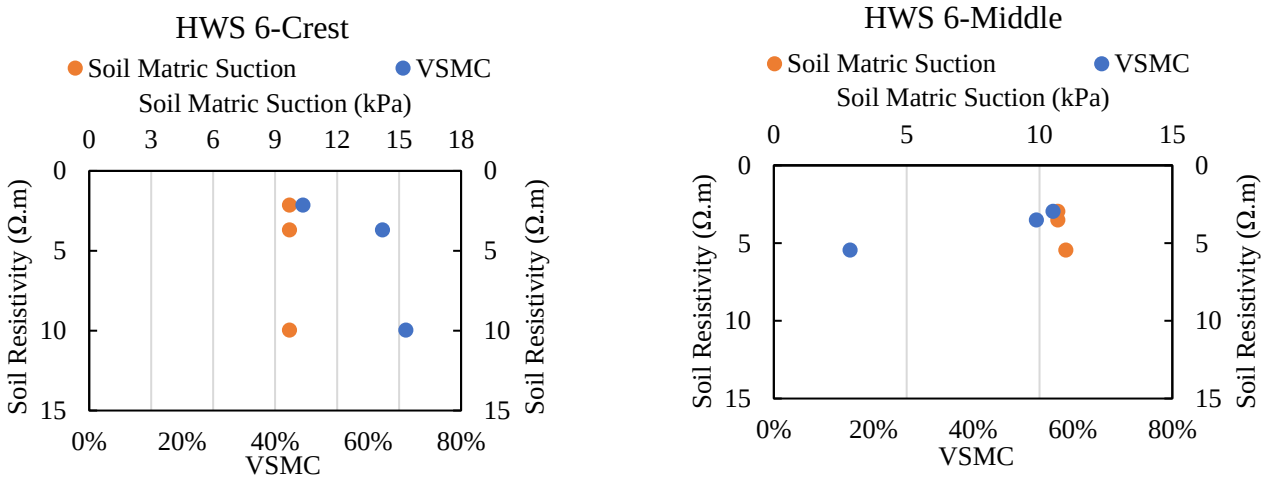

(**a**) (**b**)

Figure 31. HWS 6 comparison of 2D ERI test profile with field instrumentation (**a**) At crest of the slope (**b**) At middle of the slope (1 m = 3.28 ft; 1 mm = 0.039 in; 1 kPa = 20.89 psf).

7. Data Analysis

Data analysis was conducted for variations of ERI with VSMC and SMS and model development (2D and 3D) to identify the following dependencies and relationships amongst the geotechnical and geophysical properties of the soil:

Field Instrumentation and ERI Data

At the crest of HWS 1, 4 and 6, it was observed that the VSMC decreases with depth (Figures 9, 17 and 25). A likely explanation for this observation is that rainwater runoff from the highway is absorbed by clay in the shallow layers of the HWS's crest and takes time to percolate to the lower depths. Therefore, the upper soil layers at the crest are wetter than the deeper layers. On the other hand, in the middle of the HWS, the VSMC increases with depth. This data is corroborated up to some extent by the ERI data as well, as shown in Figures 9 and 10. The middle of the HWS is not affected by the runoff water from the highways and maintains dryer soil at the shallow levels and wetter soil at greater depths.

For almost all the HWS at the crest and middle, the SMS potential of the soil is reduced with the depth of the soil. This is understandable as the SMS potential is normally higher in unsaturated soil in the shallow depths and decreases as the degree of saturation increases. At the crest section of HWS 4 and 6 (Figures 21 and 29), it was seen that the SMS potential either remained constant or increased with depths. This observation corroborates with the observation of higher VSMC present at shallow depths at the crest compared to that of greater depths for the same HWS.

Variations of electrical resistivity with depth observed at the six HWS are presented in previous sections. The resistivity was observed to be generally higher at the shallow depths of the slope due to the presence of unsaturated clay. Resistivity up to 11 (Ω.m) was recorded on all slopes in the unsaturated zone except HWS4, which recorded much higher resistivity at depths of between 5–10 ft (1.5–3 m). This is likely due to the presence of loose unsaturated soil at the surficial levels of slope 4, which is highly resistive to electrical current. Soil disturbance can be spotted in the ERI inversion image presented in Figure 22 at surficial levels in slope 4. As the degree of saturation of the clay increases beyond the 10 ft (3 m) depth, the resistivity value decreases. The resistivity values of slope 3 and slope 4 were comparatively much lower than what was found at other slope sites at 15 ft (5 m) depth.

8. Model Analysis

8.1. Statistics

Soil Resistivity vs. VSMC—The relationship between soil resistivity and VSMC at the crest and the middle of all six HWS combined as a group is presented in Figure 32a. A laboratory test-based study on expansive clay in Texas by Kibria and Hossain [12] revealed an exponential relationship between VSMC and resistivity. Therefore, a similar model was tested for correlation between resistivity and VSMC but from field investigation data rather than those from lab tests. VSMC expressed as an exponential function is presented in Figure 32a. A linear model was also examined between resistivity and VSMC, but the exponential model provided a better correlation (determination coefficient of 0.59) between the geophysical (resistivity) and geotechnical (VSMC) parameters. The proposed one-parameter model can be expressed by Equation (6), where the soil resistivity and the VSMC are denoted as ε and δ, respectively. It should be noted the constants A_1 and A_2 are fitting parameters as 1.65 and -0.033, respectively.

$$\delta = A_1 e^{((A_2)\varepsilon)} \tag{6}$$

Soil Resistivity vs. SMS—There has rarely been any attempts in the literature to find the correlation between ERI and the SMS capacity of the unsaturated soil. In this study, a detailed analysis of instrumentation and ERI data was performed to explore the relationship between soil SMS and resistivity. The SMS potential of soil at any particular depth is normally negative or below zero. Therefore, a high SMS potential or the ability of soil particles to absorb water means the soil has a "less negative" value. A low SMS potential means a "more negative" value. In this study, all negative SMS values were transformed into positive values for the benefit of visualization.

The variations of resistivity with soil SMS at the crest and the middle of the Jackson metro HWS as a group are presented in Figure 32b. In contrast to the exponential relationship between VSMC and resistivity, a polynomial function of the second degree provided a better fit (determination coefficient of 0.67) between SMS and resistivity. The analysis resulted in the following proposed model function (one-parameter model) expressed by Equation (7), where the soil resistivity and the soil SMS are denoted as ε and ω, respectively. It should be noted that the constants B_1, B_2 and B_3 are fitting parameters as 12.04, −0.87 and 0.072, respectively.

$$\omega = B_1 - ((B_2)\,\varepsilon) + ((B_3)\,\varepsilon^2) \tag{7}$$

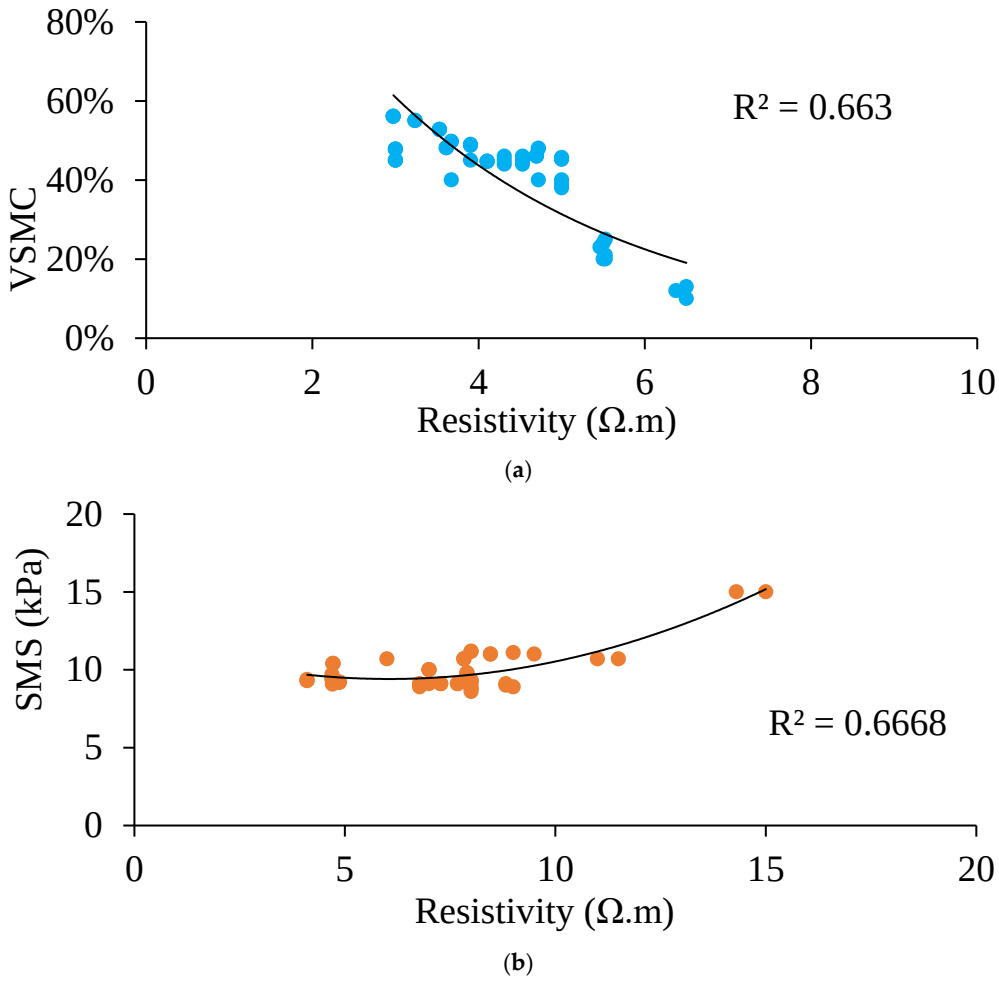

Figure 32. Variation of combined soil resistivity along with VSMC SMS of the six HWS (**a**) VSMC field-based model (**b**) SMS field-based model (1 kPa = 20.89 psf).

A 3D integrated model of the resistivity, VSMC and SMS is presented in Figure 33. The 3D plot showed that resistivity decreases as VSMC increases. On the other hand, resistivity increases while SMS increases. This symbiotic relationship between resistivity, VSMC and SMS can be very useful in inferring missing geotechnical parameters. For instance, using the predictive models developed in this study, the VSMC and SMS potential can be determined by resistivity data obtained from the non-destructive ERI test. In the presented 3D model, the soil resistivity, VSMC and soil SMS are denoted as ε, δ and ω, respectively. Then, the soil resistivity of the high expansive clay soil (HECS) of the HWS in an unsaturated two-parameter model can be described in Equation (8), where C_1, C_2, C_3 and C_4 are 3D media fitting parameters as 0 (when fixed at bound), 0.26, 24.11, 0.065 and −2.94, respectively. It

should also be noted that the goodness of fit of the proposed model is presented with an estimated coefficient of determination of 0.52 and a root mean square error of 1.6.

$$\varepsilon = C_1 + ((C_2)\,\omega) + ((C_3)\,\delta) + ((C_4)\,\omega^2) + ((C_5)\,\omega\,\delta) \quad (8)$$

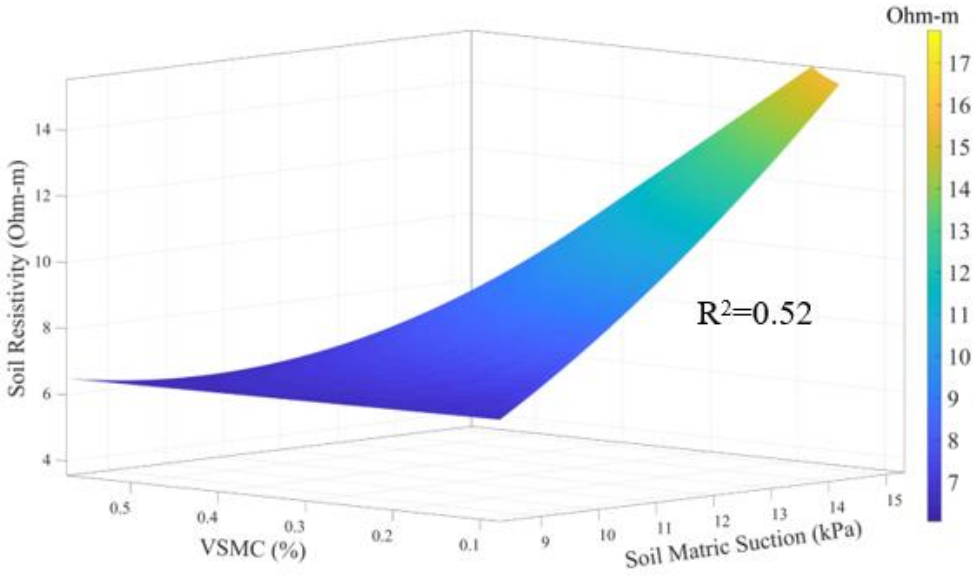

Figure 33. Three-dimensional illustration of field-based soil resistivity function (1 kPa = 20.89 psf; 1 mm = 0.0396 in).

8.2. Validation

The ERI test values and instrumentation data collected from slope 5 for June 2021 were randomly selected for model validation. These data points were not among the ones used for the model development; therefore, they provided a fair evaluation of the models. However, for the future study and current model upgrading task, different HWS other than those mentioned in this study with both field instrumentation and ERI available data will be used for model validation and verification as well. Currently, besides the six HWS considered in this study, there is no other HWS in the Jackson MS area with similar field instrumentation installed.

Figure 34 illustrate that for a given set of resistivity values at various depths, the exponential model predicted VSMC with fair accuracy, especially at the crest of the slopes. The VSMC recorded by the moisture sensor at the middle of the slopes was considerably higher than what the model predicted and therefore failed the validation test and has been excluded from the validation test. Figure 34 illustrate the capability of the developed model in predicting the SMS potential for a given set of ERI values. Five out of the six predicted SMS values were within a 10% error margin when compared with measured values, thus indicating a healthy predicting model.

To test the accuracy of the predicted models, a comparison of the predicted and measured values for VSMC is presented in Figure 35. The prediction accuracy for VSMC is good (determination coefficient of 0.86), especially for the three data points for the crest of the slopes. The middle data of the VSMC predictions have been excluded as the exponential model predicted lower VSMC values compared to the measured ones. Figure 34d shows that over 80% of predicted SMS values matched with the measured values with minimal error margins. These results inspire confidence in the developed models to predict VSMC and SMS through resistivity data obtained from the ERI investigation.

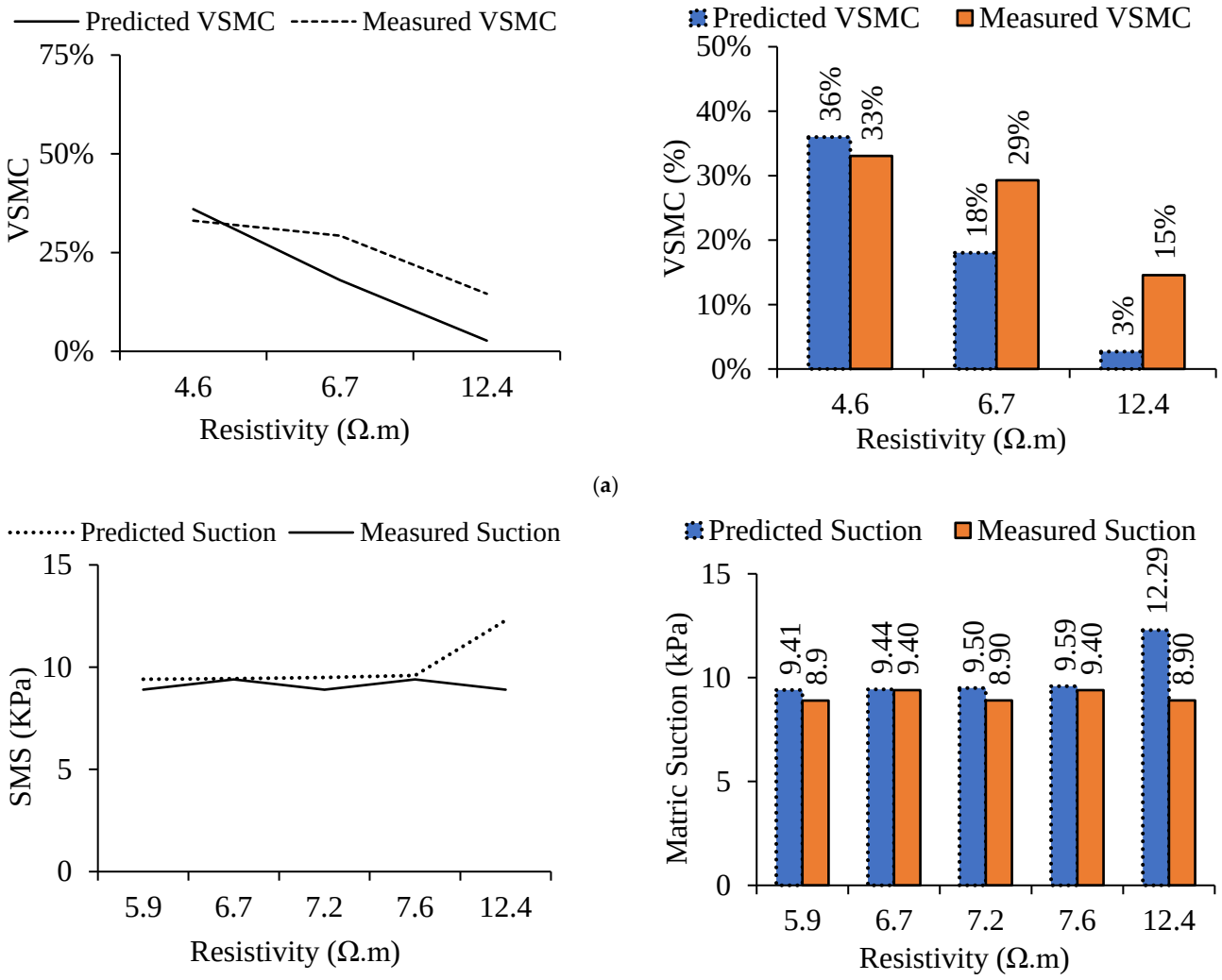

Figure 34. Validation of the developed field-based models (**a**) VSMC (**b**) SMS (1 kPa = 20.89 psf).

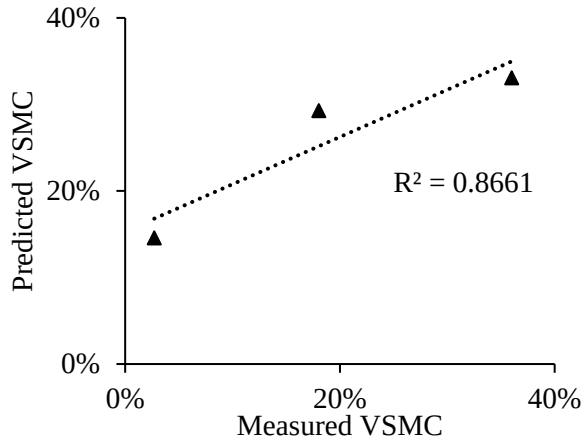

Figure 35. VSMC field-based model prediction accuracy.

9. Discussion

ER of soils and water content have an undeniable relationship [27,28] which was further put to the test in this study. However, the larger goal of this study was to explore the relationship between resistivity and SMS. Mostly because within expansive clay soils,

SMS -based assessments are critical for proper infrastructure foundation construction and embankment stability. However, models from which SMS can be inferred are scarce [29]. It will be feasible to develop the 2D SMS soil profile using a model that ties the ER to the SMS. Currently, only water potential probes can be installed in the ground to collect data on SMS changes at specific points. The 2D and 3D SMS variation inside the soil was developed for HWS constructed on expansive Yazoo clay using the ER imaging technique and a link between ERI and SMS. However, critical factors affecting soil resistivity (temperature changes, anisotropy, permittivity degree) might have contributed effectively to reduce the degree of the correlation of the model. As SMS was observed in field instrumentation data collected during the fall and summer months for the six HWS, it exhibited relatively low fluctuation in comparison to VSMC variations. This occurred as a result of the formation of shrinkage cracks caused by the highly plastic clay's shrink/swell potential and resulted in an increase in vertical permeability, which allows for more rainfall infiltration over the summer and early fall. Due to the low horizontal permeability of Yazoo clay soils, infiltrated water remained within the slope, resulting in a perched water state. Due to the presence of perched water within highway slopes containing Yazoo clay, the condition is susceptible to soil displacement within the slopes as a result of an unanticipated trend in SMS fluctuations. Based on state study 286 [3], five to seven years after construction, slope failures of highway embankments containing high expansive clays occur due to the formation of perched water conditions [3]. As a result, prospective affecting parameters were implicitly included in order to reduce the correlative models associated with SMS, and the correlation of ERI and SMS is site-specific.

In December 2020, SMS increased at the 10 ft (3 m) depth, resulting in a decrease in VSMC variation at this depth (similar to HWS 2 and 5). The only fluctuation in VSMC is detected at a depth of 5 ft (1.5 m). As was the case in the middle of the HWS, VSMC stayed constant at a depth of 15 ft (5 m) but fluctuated at a depth of 10 ft (3 m). At the midpoint of the HWS, no difference in SMS potential was observed (HWS 1, 3, 4 and 6). From January to June, VSMC ranged between 25% and 60% at all depths, then stayed stable until July and October, when rainfall was low and large changes reappeared. SMS fluctuated between 5 ft (1.5 m) and 10 ft (3 m) depths in the middle of the HWS. The VSMC fluctuated between 5 ft (1.5 m) and 15 ft (5 m). At a depth of 5 ft (1.5 m), the decrease in SMS value around September coincided with an increase in VSMC. Similarly, at a depth of 10 ft (3 m), the decrease in SMS during the middle of the HWS in July coincided with an increase in VSMC at that level. SMS remained steady throughout the HWS, but fluctuation was seen at a depth of 5 ft (1.5 m) during the fall months.

As noted in the majority of the mentioned and reviewed HWS earlier in this study, the decrease in VSMC corresponded to the summer months' decreased rainfall at six HWS. Even though the VSMC varied, there was no corresponding difference in SMS. This insight can be applied to the local soil type's features (high plastic Yazoo clay) [3] saturation level, groundwater level, fissures, voids and other environmental elements, where water infiltration and permeation patterns are site-specific and dependent on other factors such as seasonal variations. The ERI results were also a good validation of changes in VSMC and SMS at different depths and at different locations indicating and showing fully saturated condition.

It should also be mentioned that ERI has been around for many years and has been used for characterizing VSMC and even ice content in permafrost regions [30,31]. It is common knowledge that ground truth is required to calibrate the ERI models. Consequently, the models developed in this study could be translated to other areas with similar soil index properties. However, similar models developed in this study could be generated for different soil types using the technique described in this study.

10. Conclusions

Changes in VSMC and SMS impact the swelling and shrinkage behavior of expansive soil in HWS in central Mississippi. Because there is a connection between VSMC variation

and HWS performance, estimating VSMC, as well as the soil SMS of HWS, could be used to assess the early shallow movements of the HWS constructed on expansive clay soil. In situ VSMC is a key parameter that can have a substantial impact on the safety of HWS built on high plastic clay soil. ERI is a geophysical method for subsurface VSMC mapping that could be connected with VSMC and SMS of HECS to significantly improve the evaluation of HWS performance. However, there are limited datasets available to test the accuracy and practicality of the available correlative field-based models for HECS soils under varied field circumstances. Six HWS in the Jackson metropolitan region were used as reference slopes. At each of the six slopes, extensive field instrumentation was used to track VSMC, SMS and rainfall intensity. The sensors are installed at the slope's crest, middle and toe. Furthermore, a two-dimensional ERI test was carried out utilizing a dipole–dipole array with several electrodes and spacing in two survey lines at the crest and center of the six HWS to image the continuous soil subsurface profile in terms of moisture change. Based on the field instrumentation and ERI data analysis, the summary of the findings is presented below:

- Based on the field instrumentation obtained results, it was observed that during the wet season, the SMS remained consistent, ranging around −208.8 psf (−10 kPa) at three depths. The soil body of the HWS is fully saturated once the SMS variation reaches an equilibrium condition with a low value.
- Based on the ERI testing results, it was observed that shallower depths had higher resistivity values due to the existence of cracks and displaced disturbed soils.
- For combined data with all the HWS, the determination coefficient was observed to be 0.66 between ERI and both SMS and VSMC (one-parameter model).
- Based on the 3D illustrative model (two-parameter model) of soil moisture and suction obtained from the field instrumentation and field ERI testing results, it was observed that the resistivity exhibited a compatible variation with soil SMS and inverse variation with VSMC.
- Based on the field data analysis, it was found that the performance of the proposed VSMC model was satisfactory (better than the SMS performance model) as the model predictions agreed well with the field instrumentation recorded data.

Author Contributions: Conceptualization, M.S.K. and M.N.; methodology, M.S.K., R.S. and M.N.; software, R.S. and M.N.; validation, R.S.; formal analysis, R.S. and M.N.; investigation, M.S.K., R.S. and M.N.; resources, M.S.K. and F.A.; data curation, R.S. and M.N.; writing—original draft preparation, R.S. and M.N.; writing—review and editing, R.S. and M.N.; visualization, R.S. and M.N.; supervision, M.S.K.; project administration, M.S.K.; funding acquisition, M.S.K. and F.A. All authors have read and agreed to the published version of the manuscript.

Funding: The material presented in this study is based upon the work supported by the Mississippi Department of Transportation's (MDOT) State Study 286 and 316.

Institutional Review Board Statement: Not applicable.

Informed Consent Statement: Not applicable.

Data Availability Statement: The data presented in this study are available on request from the corresponding author.

Acknowledgments: The authors would like to thank and acknowledge the Mississippi Department of Transportation (MDOT). The findings, conclusions and recommendations expressed in this material are those of the authors and, necessarily, it does not reflect the viewpoints of the MDOT.

Conflicts of Interest: The authors declare no conflict of interest.

References

1. Sleep, M.D. *Analysis of Transient Seepage through Levees*; Virginia Polytechnic Institute and State University: Blacksburg, VA, USA, 2011.
2. Mahmood, K.; Kim, J.M.; Ashraf, M.; Ziaurrehman. The Effect of Soil Type on Soil Matric Suction and Stability of Unsaturated Slope Under Uniform Rainfall. *KSCE J. Civ. Eng.* **2016**, *20*, 1294–1299. [CrossRef]

3. Khan, M.S.; Amini, F.; Nobahar, M. *Performance Evaluation of Highway Slope on Yazoo Clay*; Mississippi Department of Transportation (MDOT) Federal Highway Administration (FHWA), TRID: Washington, DC, USA, 2020.
4. Azhar, A.T.; Fazlina, M.I.; Aziman, M.; Fairus, Y.M.; Azman, K.; Hazreek, Z.A. Preliminary Analysis on Soil Matric Suction for Barren Soil. Materials Science and Engineering. In *IOP Conference Series*; IOP Publishing: Bristol, UK, 2016; Volume 160, p. 012052.
5. Nobahar, M.; Khan, M.S.; Alzeghoul, O.E.; Graham, G.; Young, K. Condition Assessment of Highway Slopes Using Field Instrumentation and Electrical Resistivity Imaging (ERI). In Proceedings of the Geo-Congress 2022, Geo-Institute, ASCE, Charlotte, NC, USA, 20–23 March 2022.
6. Nobahar, M.; Khan, M.S.; Salunke, R.; Gardner, A.; Chia, H. Moisture Variation Monitoring of Failed and Not-Failed Highway Slope Through Resistivity Imaging in Mississippi. In Proceedings of the Geo-Congress 2022, Geo-Institute, ASCE, Charlotte, NC, USA, 20–23 March 2022.
7. Khan, M.S.; Nobahar, M.; Hossain, M.S.; Ivoke, J. Investigation of a Highway Slope Failure on Yazoo Clay Using Electrical Resistivity Imaging (ERI). In *Geo-Extreme*; American Society of Civil Engineers: Reston, VA, USA, 2021; pp. 255–265.
8. Abu-Hassanein, Z.S.; Benson, C.H.; Holtz, L.R. Electrical resistivity of compacted clays. *J. Geotech. Eng.* **1996**, *122*, 397–406. [CrossRef]
9. Fukue, M.; Minato, T.; Horibe, H.; Taya, N. The micro-structures of clay given by resistivity measurements. *Eng. Geol.* **1999**, *54*, 43–53. [CrossRef]
10. Samouëlian, A.; Cousin, I.; Tabbagh, A.; Bruand, A.; Richard, G. Electrical resistivity survey in soil science: A review. *Soil Tillage Res.* **2005**, *83*, 173–193. [CrossRef]
11. Giao, P.; Chung, S.; Kim, D.; Tanaka, H. Electric imaging and laboratory resistivity testing for geotechnical investigation of Pusan clay deposits. *J. Appl. Geophys.* **2003**, *52*, 57–175. [CrossRef]
12. Kibria, G.; Hossain, M.S. Investigation of Geotechnical Parameters Affecting Electrical Resistivity of Compacted Clays. *J. Geotech. Geoenv.* **2012**, *138*, 1520–1529. [CrossRef]
13. Archie, G. *The Electrical Resistivity Log as an Aid in Determining Some Reservoir Characteristics*; Petroleum Technology, T.P. 1422; Shell Oil Co.: Houston, TX, USA, 1942.
14. Sauer, M.C.; Southwick, P.F.; Spiegler, K.S.; Wyllie, M.R.J. Electrical conductance of porous plugs-ion exchange resin-solution systems. *Ind. Eng. Chem.* **1955**, *47*, 2187–2193. [CrossRef]
15. Waxman, M.H.; Smits, L.J.M. Electrical conductivity in oil bearing shaly sands. *Soc. Pet. Eng. J.* **1968**, *8*, 107–122. [CrossRef]
16. Shah, P.; Singh, D. Generalized Archie's law for estimation of soil electrical conductivity. *J. ASTM Int.* **2005**, *2*, 1–19.
17. Uchimuraa, T.; Towhata, I.; Wang, L.; Nishieb, S.; Yamaguchi, H.; Seko, I.; Qiao, J. Precaution and early warning of surface failure of slopes using tilt sensors. *Soils Found.* **2015**, *55*, 1086–1099. [CrossRef]
18. Zha, F.S.; Liu, S.Y.; Du, Y.J.; Cui, K.R. The electrical resistivity characteristics of unsaturated clayey soil. *Rock Soil Mech.* **2007**, *28*, 1671–1676.
19. Piegari, E.; Maio, R.D. Estimating soil suction from electrical resistivity. *Nat. Hazards Earth Syst. Sci.* **2013**, *13*, 2369–2379. [CrossRef]
20. De Vita, P.; Di Maio, R.; Piegari, E. A study of the correlation between electrical resistivity and matric suction for unsaturated ash-fall pyroclastic soils in the Campania region (southern Italy). *Environ. Earth Sci.* **2012**, *67*, 787–798. [CrossRef]
21. Hu, Y.; Azam, S. Instrumentation for field monitoring in expansive soils. In Proceedings of the 61st Canadian Geotechnical Conference, Edmonton, AB, Canada, 21–24 September 2008.
22. Hu, Y.; Vu, H.Q.; Lotfian, K. Instrumentation of a section of AC pipe in expansive soil. In Proceedings of the Pipelines Conference 2008: Pipeline Asset Management: Maximizing Performance of our Pipeline Infrastructure, Atlanta, GA, USA, 22–27 July 2008; pp. 1–10.
23. Zhan, T.L.; Ng, C.W.; Fredlund, D.G. Instrumentation of an unsaturated expansive soil slope. *Geotech. Test. J.* **2007**, *30*, 1641.
24. Zapata, C.E.; Houston, W.N. *Calibration and Validation of the Enhanced Integrated Climatic Model for Pavement Design*; Transportation Research Board, TRID: Washington, DC, USA, 2008; Volume 602.
25. Nobahar, M. An Early Warning Protocol against Highway Slopes Failure on Expansive Soil. Ph.D. Dissertation, Jackson State University, Jackson, MI, USA, 1 May 2022.
26. Lesparre, N.; Nguyen, F.; Kemna, A.; Robert, T.; Hermans, T.; Daoudi, M.; Flores-Orozco, A. A new approach for time-lapse data weighting in electrical resistivity tomography. *Geophysics* **2017**, *82*, E325–E333. [CrossRef]
27. Muñoz-Castelblanco, J.A.; Pereira, J.M.; Delage, P.; Cui, Y.J. The influence of changes in water content on the electrical resistivity of a natural unsaturated loess. *ASTM Geotech. Test. J.* **2012**, *35*, 11–17.
28. Hen-Jones, R.; Hughes, P.; Stirling, R.; Glendinning, S.; Chambers, J.; Gunn, D.; Cui, Y. Seasonal effects on geophysical–geotechnical relationships and their implications for electrical resistivity tomography monitoring of slopes. *Acta Geotech.* **2017**, *12*, 1159–1173. [CrossRef]
29. Vann, J.; Houston, S. Field Soil Suction Profiles for Expansive Soil. *J. Geotech. Geoenviron. Eng.* **2021**, *147*, 04021080. [CrossRef]
30. You, Y.; Yu, Q.; Pan, X.; Wang, X.; Guo, L. Application of electrical resistivity tomography in investigating depth of permafrost base and permafrost structure in Tibetan Plateau. *Cold Reg. Sci. Technol.* **2013**, *87*, 19–26. [CrossRef]
31. Hoekstra, P.; Sellmann, P.V.; Delaney, A. Ground and airborne resistivity surveys of permafrost near Fairbanks, Alaska. *Geophysics* **1975**, *40*, 641–656. [CrossRef]